Dynamical Climatology

The adjustment of numerical weather prediction models to local perturbations.

by

B.R. Barwell and R.A. Bromley

DCTN 56

April 1987

Meteorological Office (Met. O. 20)
London Road
Bracknell
Berkshire RG12 2SZ

DYNAMICAL CLIMATOLOGY TECHNICAL NOTE NO. 56

THE ADJUSTMENT OF NUMERICAL WEATHER PREDICTION MODELS TO LOCAL PERTURBATIONS

by

B R Barwell and R A Bromley

Met O 20 (Dynamical
Climatology Branch)
Meteorological Office
London Road
Bracknell
Berkshire RG12 2SZ U.K.

April 1987

(with corrections Nov. 1987)

Note: This paper has not been published. Permission to quote from it should be obtained from the Assistant Director of the above Meteorological Office branch.

SUMMARY

The linearised two-dimensional equations of motion on an f-plane are solved for a localised perturbation using local polar co-ordinates, and a general solution involving Bessel functions is found which can be fitted to any initial conditions. Three types of perturbation are used as examples; they show the formation of an external gravity wave which propagates outward leaving a geostrophically balanced residual flow as $t \to \infty$. The divergent component of the initial wind field has no effect on this residual flow. Experiments in which the same perturbations were applied to all levels of a numerical model showed good agreement with the analytical solutions.

Using an isentropic temperature profile as an example, the theory is extended to three dimensional perturbations. As well as the gravity waves and geostrophic residual flow found in two dimensions, a third component of the solution is found, namely, an inertial oscillation originating in the deviation of the wind perturbation from its vertical mean. This oscillation continues indefinitely with the coriolis frequency. Numerical model experiments show good agreement with the solutions in the early stages of adjustment though the inertial oscillation slowly decays through internal gravity waves.

Finally, the analytical solutions are discussed in the light of the results of research on the design and performance of analysis schemes.

1. Introduction

The atmosphere is in a state of approximate balance. Although the circulation pattern is constantly changing, high frequency processes which could theoretically occur in the atmosphere form an insignificant part of its variability. In the absence of this activity, the assumption of geostrophic or gradient balance between height and wind fields is frequently assumed.

Numerical models of the general circulation succeed in modelling and maintaining this state of approximate balance throughout long periods of integration. However, the process of numerical weather prediction requires that input from available observational data be assimilated into models to provide the best possible starting analysis. Unless special care is taken, data assimilation can introduce spurious high frequency gravity wave noise into numerical models. Although this noise has little interaction with meteorologically significant activity, its existence implies loss of part of the information contributed by the observational data. The problem is especially important for the process of intervention in which a human forecaster attempts to cause changes in the analysis in order to improve forecasting ability. This is frequently done when an isolated but good quality observation is liable to be rejected by the model's quality control procedure, or where the forecaster knows from other sources that the analysis is poor.

Much attention has been given to methods of suppressing the generation of high frequency gravity wave noise. Techniques include multivariate analysis schemes, initialization, and repeated insertion of data. Daley (1980) has discussed the problem of the optimal initial conditions for forecast models in the light of the slow manifold of Leith (1980).

In this paper we study the adjustment process using a simple linearised two-dimensional f-plane model subjected to isolated perturbations of its initial static state. A simpler one-dimensional problem was solved by Cahn (1945) for initial conditions first proposed by Rossby. Further work in this field was reviewed by Blumen (1972). A more

general solution of the one-dimensional problem for continuous and discrete cases was given by Arakawa (1984). Cahn's one-dimensional solution involved the Bessel function J_0. Formulae involving Bessel functions have also been proposed for the horizontal correlation of forecast errors in height fields (Balgovind et al 1983) and, more recently for both height and wind errors (Hollingsworth and Lönnberg 1986, Lönnberg and Hollingsworth 1986). The analysis in the present paper also leads to solutions involving Bessel functions.

Gill (1980) investigated solutions to the shallow water equations on a β-plane with local diabatic heating in the tropics. The solutions, which involve parabolic cylinder functions reflect some features of the tropical atmospheric circulation. Heckley and Gill (1984) found transient solutions for the case where the heating is suddenly switched on, and discovered that several days were necessary for a steady state to be reached.

The requirements of a theory to describe the adjustment process for a local perturbation differ from those for tropical heating. The effect of a single observation covers a relatively small area and decreases during forecasts as model errors grow and eventually dominate. Thus we are interested in smaller spatial scales and shorter time scales than for the tropical heating problem. For this reason we choose an f-plane rather than a β-plane for our analysis. We consider perturbations in extra-tropical latitudes where the f-plane can usefully be applied for spatial scales of about 1000 kilometres. Even in the tropics however, the theory is not seriously invalidated because the coriolis term is small and does not have much effect on the flow on the time scales in which we are interested.

Since we focus attention on short time scales, it is necessary to determine the transient as well as the steady state solution. This is important for assimilation schemes involving repeated insertion of data since significant transient processes occur on time scales less than the period over which the data is inserted. A transient solution will necessarily involve a mathematical description of the formation and propagation of external gravity waves during the adjustment.

External gravity waves are those whose phase is independent of the vertical co-ordinate. Solutions of the shallow water equations include those representing the propagation of these gravity waves which correspond to surface waves on water. In contrast, internal gravity waves have a more complex vertical structure which cannot be represented in a two-dimensional model. However, with analysis schemes typical of those used in numerical models, most of the initial gravity wave activity is in the form of external gravity waves. Internal waves typically take several assimilation cycles before they grow to a size which limits the application of solutions from a two-dimensional model. Both forms of gravity waves represent transient activity which eventually subsides leaving a residual, meteorologically significant component of the flow.

Using a simple analytical f-plane model, Barwell and Lorenc (1985) investigated the behaviour of single-wavelength wind perturbations periodic in both x- and y-directions. The solution for such cases is equivalent to solving the linearised equations using the method of separation of variables with Cartesian co-ordinates in the f-plane. They found that in the early stages of the evolution, the perturbation decays more slowly if only the rotational component of the wind is perturbed or if a geostrophically balancing height perturbation is also applied. These results were supported by studies of the evolution of local perturbations in a global general circulation model.

A solution that is periodic in x and y represents the decay of a local perturbation only up to the time taken for gravity waves to travel the repeat distance since thereafter, each centre is influenced by waves from its neighbours. A better representation could be made using a Fourier spectrum of periodic solutions fitted to a more complicated initial state (Tanaka 1984). However, for a perturbation localised about a central point, a more suitable representation can be achieved using local polar rather than Cartesian co-ordinates.

In this paper we solve the two-dimensional equations of motion linearised about a static mean state using the technique of separation of variables, and polar co-ordinates in the horizontal plane. This leads to

solutions involving Bessel functions of the first kind which can be fitted to the initial state. Furthermore, the fitting can be performed analytically for some instructive and realistic perturbations based on a Gaussian horizontal form. The general theory is presented in the next section. Section 3 illustrates the solutions using three special cases; a zonal wind perturbation, a non-divergent wind perturbation and a height perturbation. In section 4, these three cases are compared with the response of a global forecast model to similar perturbations. Section 5 investigates the long term response of the analytical solutions. The theoretical analysis is extended in section 6 to the case of a perturbation applied through a limited depth of the atmosphere. Solutions are found for the wind perturbations used in section 3 and are compared with equivalent numerical model experiments. Results are discussed in the light of the properties of data assimilation schemes in section 7, and a summary of our findings is presented in section 8.

2. Linearised Adjustment Theory

a. Basic equations

Consider a perturbation applied to an atmosphere initially at rest and with uniform depth H. The two-dimensional equations of motion and continuity linearised about this static state on an f-plane are the shallow water equations,

$$\frac{\partial u}{\partial t} - fv + \frac{\partial \phi}{\partial x} = 0, \tag{1}$$

$$\frac{\partial v}{\partial t} + fu + \frac{\partial \phi}{\partial y} = 0, \tag{2}$$

$$\frac{\partial \phi}{\partial t} + \Phi\left(\frac{\partial u}{\partial x} + \frac{\partial v}{\partial y}\right) = 0. \tag{3}$$

Here $\Phi = gH$ is the mean geopotential, and ϕ, u and v are perturbations of the geopotential and wind component fields about the initial state. In addition to the static state, these equations can also be considered valid for an initial state of uniform flow with the velocity components expressed relative to a co-ordinate system advected with the mean velocity. The steady state solutions of Eqs. (1)-(3), found by setting the time derivatives to zero represent geostrophically balanced flows. An unbalanced perturbation must therefore evolve towards a balanced final state. It is convenient to express the equations in terms of the divergence D and vorticity α of the ageostrophic component of the wind field; these quantities must then decay to zero as $t \to \infty$. α is related to the total vorticity ζ by the definition

$$\alpha = \zeta - \frac{1}{f} \nabla^2 \phi . \tag{4}$$

Introducing D and ζ in place of u and v, Eqs. (1)-(3) become

$$\frac{\partial D}{\partial t} - f \zeta + \nabla^2 \phi = 0, \tag{5}$$

$$\frac{\partial \zeta}{\partial t} + f D = 0, \tag{6}$$

$$\frac{\partial \phi}{\partial t} + \Phi D = 0. \tag{7}$$

Substituting α for ζ from Eq. (4), Eq. (5) becomes

$$\frac{\partial D}{\partial t} - f \alpha = 0. \tag{8}$$

Solving the system of equations (5)-(7) for the divergence yields (Arakawa 1984)

$$\frac{\partial^2 D}{\partial t^2} + f^2 D - \Phi \nabla^2 D = 0. \qquad (9)$$

In view of Eq. (8), this equation also holds if D is replaced by α .

b. Solution for a localised perturbation

To solve Eq. (9) for a localised perturbation, we use polar co-ordinates and search for solutions of the form F(r,t) sin nθ or F(r,t) cos nθ. The method of separation of variables shows that if r and t are separable, Bessel function solutions exist of the form

$$J_n(kr) \sin\left(f^2 + k^2\Phi\right)^{1/2} t \sin n\theta, \qquad (10)$$

together with corresponding cosine forms. The constant k may have any real value. As well as solutions involving Bessel functions of the first kind, $J_n(kr)$, similar forms involving Bessel functions of the second kind, or modified Bessel functions (corresponding to imaginary k) also exist but must be rejected for the present problem because of singularities at zero or infinite r. All forms of the expressions (10) are eigensolutions of the equation

$$\nabla^2 D + k^2 D = 0. \qquad (11)$$

Since equations (5) to (7) are linear, more complex solutions can be generated by combining terms of the form (10). In the general case, this involves a summation over integer values of n and an integration over all positive k. Taking the sine and cosine forms for the trigonometric functions gives a four-term general solution

$$D = \sum_{n=0}^{\infty} \int_{0}^{\infty} \left[P_n(k) \cos \omega_k t \cos n\theta + Q_n(k) \sin \omega_k t \cos n\theta \right.$$

$$\left. + R_n(k) \cos \omega_k t \sin n\theta + S_n(k) \sin \omega_k t \sin n\theta \right] J_n(kr)\, dk \quad (12)$$

where

$$\omega_k^2 = f^2 + k^2 \Phi , \quad (13)$$

and the functions $P_n(k)$, $Q_n(k)$, $R_n(k)$ and $S_n(k)$ are to be determined from the initial conditions as described below.

The general solution (12) is easily expressed in the more familiar form of height and wind fields. A term-by-term integration with respect to time gives the geopotential field ϕ according to Eq. (7) which in turn determines the height field. By Eq. (6), a similar integration also determines the vorticity field. The divergence and vorticity fields are easily converted to velocity potential and stream function (using Eq. (11) and the equivalent equation for α) from which the wind components u and v can be derived. The calculation is straightforward and can be performed quite generally, but the algebra is complicated. Rather than present the general formulae, the special cases treated in section 3 will illustrate the calculation.

c. Boundary conditions

The coefficients $P_n(k)$, $Q_n(k)$, $R_n(k)$ and $S_n(k)$ in Eq. (12) can be determined for a given initial perturbation by fitting the divergence $D(r,\theta,t)$ and ageostrophic vorticity $\alpha(r,\theta,t)$ at t=0. From Eq. (12),

$$D(r,\theta,0) = \sum_{n=0}^{\infty} \int_0^{\infty} \left(P_n(k) \cos n\theta + R_n(k) \sin n\theta \right) J_n(kr)\, dk, \qquad (14a)$$

and similarly, using Eq. (9) we find

$$\alpha(r,\theta,0) = \sum_{n=0}^{\infty} \int_0^{\infty} \left(Q_n(k) \cos n\theta + S_n(k) \sin n\theta \right) \omega_k J_n(kr)\, dk. \qquad (14b)$$

The inversion of these two equations is accomplished by means of a Fourier analysis in θ and the appropriate Bessel function transform (Hankel transform) in r. For n=0 the results are

$$\left.\begin{aligned} P_0(k) &= \frac{k}{2\pi} \int_0^{\infty} \int_0^{2\pi} D(r,\theta,0)\, r J_0(kr)\, dr\, d\theta, \\ Q_0(k) &= \frac{fk}{2\pi\omega_k} \int_0^{\infty} \int_0^{2\pi} \alpha(r,\theta,0)\, r J_0(kr)\, dr\, d\theta, \\ R_0(k) &= S_0(k) = 0, \end{aligned}\right\} \qquad (15)$$

and for n>0,

$$
\left.
\begin{aligned}
P_n(k) &= \frac{k}{\pi} \int_0^{\infty} \int_0^{2\pi} D(r,\theta,0)\, r\, J_n(kr) \cos n\theta \, dr \, d\theta, \\
Q_n(k) &= \frac{fk}{\pi \omega_k} \int_0^{\infty} \int_0^{2\pi} \alpha(r,\theta,0)\, r\, J_n(kr) \cos n\theta \, dr \, d\theta, \\
R_n(k) &= \frac{k}{\pi} \int_0^{\infty} \int_0^{2\pi} D(r,\theta,0)\, r\, J_n(kr) \sin n\theta \, dr \, d\theta, \\
S_n(k) &= \frac{fk}{\pi \omega_k} \int_0^{\infty} \int_0^{2\pi} \alpha(r,\theta,0)\, r\, J_n(kr) \sin n\theta \, dr \, d\theta.
\end{aligned}
\right\} \qquad (16)
$$

In simple cases the integrals involved in these equations can be performed analytically using tables of integral transforms (eg Erdélyi 1954) as in the examples in the following section.

3. Examples

To illustrate the application of the theory, we will consider three cases of local perturbations: (a) a perturbation in the zonal wind, (b) a non-divergent wind perturbation and (c) a height perturbation. In each case, the form of the initial perturbation is based on a Gaussian function like that commonly assumed to represent horizontal correlation functions in numerical models. The three cases are illustrated in Fig. 1.

Because of the Gaussian form of these perturbations, the solutions involve integrals of similar form which will be denoted by the shorthand notation:

$$A_{l,m}(r,t) = fd \int_0^\infty \frac{(kd)^l}{\omega_k} J_m(kr) \sin \omega_k t \exp\left(-\tfrac{1}{2}k^2d^2\right) dk , \tag{17}$$

$$B_{l,m}(r,t) = f^2d \int_0^\infty \frac{(kd)^l}{\omega_k^2} J_m(kr) \left(1-\cos \omega_k t\right) \exp\left(-\tfrac{1}{2}k^2d^2\right) dk , \tag{18}$$

where d is a constant representing the horizontal scale of the perturbation. The rapid decay of the exponential function allows the integrals to be evaluated numerically without difficulty. The factors outside the integrals make the expressions dimensionless.

a. Zonal wind perturbation

This case, illustrated in Fig. 1(a) is described by

$$u(r,\theta,0) = U \exp\left(-r^2/2d^2\right) , \quad v(r,\theta,0) = 0 , \quad \phi(r,\theta,0) = 0 \tag{19}$$

where U is the magnitude of the wind at the origin (centre of perturbation) and d the distance at which the wind falls to $e^{0.5}$ (=0.607) of its central value. In terms of divergence and ageostrophic vorticity, Eqs. (19) become

$$\left.\begin{aligned} D(r,\theta,0) &= -\frac{U}{d^2} r\cos\theta \exp\left(-r^2/2d^2\right), \\ \zeta(r,\theta,0) &= \frac{U}{d^2} r\sin\theta \exp\left(-r^2/2d^2\right). \end{aligned}\right\} \tag{20}$$

Evaluating $P_n(k)$, $Q_n(k)$, $R_n(k)$ and $S_n(k)$ from Eqs. (15) and (16),

$$P_1(k) = -k^2 d^2 U \exp(-\tfrac{1}{2}k^2 d^2), \qquad S_1(k) = \frac{f}{\omega_k} k^2 d^2 U \exp(-\tfrac{1}{2}k^2 d^2), \tag{21}$$

all other coefficients being zero. Substituting in Eq. (12) and integrating Eq. (6) yields the geopotential field

$$\phi(r,\theta,t) = \frac{\bar{\Phi} U}{fd}\left(A_{2,1}(r,t)\cos\theta - B_{2,1}(r,t)\sin\theta\right), \tag{22}$$

and the wind component fields evaluated as described in the previous section are

$$u(r,\theta,t) = U\left(\exp(-r^2/2d^2) - B_{1,0}(r,t)\right)$$

$$- \frac{U\bar{\Phi}}{2f^2d^2}\left(B_{3,0}(r,t) - B_{3,2}(r,t)\cos 2\theta\right), \tag{23}$$

$$v(r,\theta,t) = -UA_{1,0}(r,t) + \frac{U\bar{\Phi}}{2f^2d^2} B_{3,2}(r,t)\sin 2\theta. \tag{24}$$

As an illustration, consider a perturbation of the form given in Eq. (19) (Fig. 1a) with U=10 m/s and d=400 km. We use a value of f appropriate for latitude 38.25°N and an equivalent depth H=Φ/g=8485.38 m which may be regarded as appropriate for an atmosphere with a surface temperature of 290°K (see Eq. 45, section 6). Figs. 2(a) to 2(d) show stages in the evolution of the perturbation after 1, 2, 3 and 6 hours as given by Eqs. (22) to (24). The illustrations show how the height field, which is rapidly generated by the divergence of the initial perturbation, develops into a gravity wave which propagates outward leaving a residual flow with reduced

intensity. After six hours the gravity wave has separated from the residual flow which quickly settles into a geostrophically balanced double-vortex pattern. The wind speed at the centre of this residual is less than half that of the initial perturbation (see section 5). Applied to the problem of assimilating wind data, the gravity wave represents spurious noise which may be removed by initialization or other techniques. The residual flow represents the component of the perturbation which is retained by the model and appears as a local influence in forecasts.

b. Non-divergent wind perturbation

We now consider the non-divergent wind perturbation shown in Fig. 1(b) given by

$$\left.\begin{aligned} u(r,\theta,0) &= U\left(1-\frac{r^2}{d^2}\sin^2\theta\right)\exp\left(-r^2/2d^2\right), \\ v(r,\theta,0) &= \frac{Ur^2}{2d^2}\sin 2\theta\,\exp\left(-r^2/2d^2\right), \\ \phi(r,\theta,0) &= 0. \end{aligned}\right\} \qquad (25)$$

U and d have the same significance as in section 3(a). The divergence of this field is zero everywhere and the ageostrophic component of vorticity is

$$\zeta(r,\theta,0) = \frac{Ur}{d^2}\left(4-\frac{r^2}{d^2}\right)\sin\theta\,\exp\left(-r^2/2d^2\right). \qquad (26)$$

The coefficients in Eqs. (15) and (16) are all found to be zero except $S_1(k)$ which has the value

$$S_1(k) = \frac{f}{\omega_k} k^4 d^4 U \exp\left(-\tfrac{1}{2}k^2 d^2\right). \tag{27}$$

From Eq. (12), the geopotential field is given by

$$\phi(r,\theta,t) = -\frac{\Phi U}{fd} B_{4,1}(r,t) \sin\theta, \tag{28}$$

and the wind components are

$$u(r,\theta,t) = U\left(1 - \frac{r^2}{d^2}\sin^2\theta\right)\exp\left(-r^2/2d^2\right)$$

$$-\tfrac{1}{2}U\left(B_{3,0}(r,t) + B_{3,2}(r,t)\cos 2\theta - A_{3,2}(r,t)\sin 2\theta\right), \tag{29}$$

$$v(r,\theta,t) = \frac{Ur^2}{2d^2}\sin 2\theta \exp\left(-r^2/2d^2\right) \tag{30}$$

$$-\tfrac{1}{2}U\left(A_{3,0}(r,t) + A_{3,2}(r,t)\cos 2\theta + B_{3,2}(r,t)\sin 2\theta\right).$$

Figs. 3(a) to 3(c) show the evolution of the non-divergent perturbation of Fig. 1(b) after 1, 2 and 4 hours as given by Eqs. (28) to (30). The values of U, d, f and Φ used are the same as in section 3(a). Adjustment takes place more rapidly than for the zonal wind perturbation (Fig. 2), and the gravity wave is emitted in a direction perpendicular to the initial direction of the wind at the centre of the perturbation. The amplitude of the gravity wave is significantly less than in Fig. 2. A greater portion of the energy of the perturbation is therefore retained in the residual flow and the reduction in wind velocity at the centre is small.

c. Height perturbation

As a third example we consider the simple height perturbation shown in Fig. 1(c) which has the form

$$\phi(r,\theta,0) = gh\exp(-r^2/2d^2), \qquad u(r,\theta,0) = v(r,\theta,0) = 0, \tag{31}$$

where h is the magnitude of the height perturbation at its centre. The initial values of D and α are

$$\left.\begin{aligned} D(r,\theta,0) &= 0, \\ \alpha(r,\theta,0) &= \frac{gh}{fd^2}\left(2-\frac{r^2}{d^2}\right)\exp(-r^2/2d^2). \end{aligned}\right\} \tag{32}$$

Substituting in Eqs. (15) and (16), all coefficients are found to be zero except

$$Q_0(k) = \frac{gh\,k^3d^2}{\omega_k}\exp\left(-\tfrac{1}{2}k^2d^2\right), \tag{33}$$

which gives the geopotential field

$$\phi(r,\theta,t) = gh\left(\exp(-r^2/2d^2) - \frac{\Phi}{f^2d^2}B_{3,0}(r,t)\right). \tag{34}$$

The expressions for the wind components can be combined into a complex velocity

$$u(r,\theta,t) + iv(r,\theta,t) = \frac{gh}{fd}\left(A_{2,1}(r,t) - iB_{2,1}(r,t)\right)e^{i\theta} \qquad (35)$$

Using a value of 100 m for h, the evolution of the perturbation as given by Eqs. (34) and (35) after 1, 2, 3 and 6 hours is shown in Fig. 4. The centre of the perturbation quickly collapses, changing sign within an hour. A gravity wave is emitted radially outwards, taking with it most of the perturbation energy and leaving a very weak residual circulation. During this process there is very little response in the wind field to changes in the height field.

d. General comments

In all the above examples, the flow separates into two components; an outward-propagating gravity wave and a geostrophically balanced residual flow. With the physical parameters that have been used here, the separation is essentially complete within 6 hours. The external gravity wave appears as an isolated wave rather than a wave train. Its magnitude and the direction in which its energy is propagated depend on the form of the initial perturbation.

As mentioned in the introduction, a limitation of a two-dimensional model such as the one developed in section 2 is that it cannot represent any internal vertical structure in the atmospheric temperature profile and is therefore incapable of generating or maintaining internal gravity waves. The external gravity waves in Figs. 2 to 4 represent the only process by which a perturbation can decay in two-dimensional theory, and the large equivalent depth we have used is appropriate for this process. The construction of a full three-dimensional theory able to model internal gravity waves is outside the scope of this paper. However, since decay through internal gravity waves is a slower process than through the external wave, a two-dimensional theory is capable of representing the early stages of the flow. The next section illustrates the response of a

numerical model to the three perturbations of Fig. 1. This will illustrate how far the theoretical examples of this section represent the behaviour of such a model and will allow comparison with previous theory and experiments.

4. Numerical model experiments

In this section, we compare the theoretical results of section 3 with the effect of applying the perturbations of Fig. 1 to a general circulation model. Some similar experiments were performed by Barwell and Lorenc (1985) but the present work uses a more advanced numerical model with greater resolution.

The model used is a recent version of the UK Meteorological Office's operational forecast model (Bell 1983). This is a global primitive equation model on 15 unequally spaced sigma levels extending into the lower stratosphere. The model has a horizontal resolution of 1.5° latitude by 1.875° longitude and contains parametrization of physical processes such as convection, radiation etc. Further details of the model are given by Gadd (1985).

The initial conditions for the experiments were taken from a five-day forecast valid at 12 GMT 26 May 1985. The use of a forecast rather than an analysis ensures that any gravity wave noise generated by data assimilation has been damped out. Divergence damping is applied to achieve this but is discontinued after the first 6 hours of a forecast: hence it was not in operation during the runs to be described.

In separate experiments, the perturbations of Fig. 1 were applied to the five-day forecast in an area centred on 38.25°N 150.94°W (one of the model grid points). This location was chosen because it was free from major synoptic activity and topographic influences, and away from large horizontal or vertical wind gradients. Each perturbation was applied with equal magnitude at every level of the model without using any

initialization or repeated insertion technique. 18-hour forecasts were run from each of the three perturbed states as well as a control run from the unperturbed state.

Figures 5 to 7 show the differences in the height and wind fields between each of the three perturbation runs and the control run. The times, horizontal scales and contour intervals are the same as those of the corresponding Figs. 2 to 4. Figs. 5 to 7 show differences at the 500 mb level: at other levels the behaviour is similar. The similarity between these figures and Figs. 2 to 4 shows that, for at least the first six hours, the theory describes the main features of the adjustment process well, especially the formation and propagation of the gravity waves. In the f-plane model, the gravity waves continue to propagate outwards with steadily decreasing amplitudes. In the numerical model, the waves travel round the earth reaching a point diametrically opposite the location of the original perturbation at the end of the 18-hour forecast.

The theory predicts that the double-vortex patterns of Figs. 5 and 6 should be of equal intensity, but the figures show that the low is more intense than the high. The asymmetry, which does not extend to the wind field, is due to the curvature of the flow. The flow tends towards gradient balance rather than the geostrophic balance predicted by linearised theory. Failure to allow for curvature effects in multivariate analysis schemes can introduce imbalance in analyses (Williamson et al. 1981). In the present case however, the effect is not large.

For the residual flow, the similarity between theory and experiment continues beyond 6 hours. The double vortex patterns set up in Figs. 5 and 6 are clearly detectable to the end of the 18-hour forecasts. By this time, some internal gravity waves have formed and non-linear processes have distorted the pattern, but the intensity of the vortices has not been greatly reduced. Figure 8 shows the ratio of the maximum wind (or height for Figs. 4 and 7) at the centre of the perturbation to the initial value plotted against time for the first 10 hours. Full lines are theoretical curves from the equations of section 3 with r=0, and symbols represent values from the corresponding numerical model runs. There is general

agreement between model runs and theory, especially in predicting the value at which the flow settles after the initial adjustment of the first few hours. Internal gravity wave processes in the model runs do not affect the agreement until the first signs of further decay appear at about 10 hours. The theory therefore satisfactorily predicts the initial adjustment phase, the generation of external gravity waves and the subsequent behaviour of the numerical model for at least 10 hours, and with gradually decreasing accuracy thereafter.

Barwell and Lorenc (1985) investigated solutions of the shallow water equations (Eqs. (1) to (3)) for periodic perturbations with a single horizontal wavelength. Much smaller equivalent depths were chosen than that used for the examples of section 3. This was done to reduce the coupling between height and wind fields to levels more representative of perturbations applied through a limited depth of a numerical model. However, as a lower equivalent depth also reduces the speed of propagation of the external gravity waves, the solutions represent the adjustment process quantitatively only for the short period before the gravity waves have formed. To extend the application of a two-dimensional theory to the case of a perturbation of limited depth, it is necessary to preserve the large equivalent depth appropriate to external gravity waves in the atmosphere without an excessive coupling between height and wind fields. A method of achieving this is presented and assessed in section 6. It will become apparent there that the theory and experiments already described are relevant to this extended problem as well.

5. Limiting flow as $t \to \infty$

A further problem with the spatially periodic solutions studied by Barwell and Lorenc (1985) is that the height field at one perturbation is quickly contaminated by gravity waves from its neighbours. For a solution with a wavelength of 3000 km and a typical external gravity wave speed of 300 ms^{-1}, contamination will occur in about 3 hours. The result is an oscillatory solution in which the flow returns to the initial state within a time of $2\pi/f$ and thereafter oscillates indefinitely with unchanged amplitude.

This behaviour is not characteristic of an isolated perturbation in a model and precludes the calculation of a state which the flow approaches asymptotically as $t \to \infty$. By adding a divergence damping term to the linearised equations, Temperton (1973) found a steady-state flow pattern whose stream function was a linear combination of that of the initial wind field, and a hypothetical stream function in geostrophic balance with the initial height field. For large equivalent depths, the initial mass field adjusts to the wind field; for small equivalent depths, the wind field adjusts to the mass field.

The theory developed in this paper allows calculation of a limiting steady-state flow without the need for divergence damping. Instead, the transient component of the flow is dispersed by the outward propagating external gravity wave. The limiting flows for the perturbations of Fig. 1 are shown in Fig. 9. These can be computed from the formulae of section 3 given that as $t \to \infty$, the integral (17) can be shown to vanish and (18) becomes

$$B_{l,m}(r,\infty) = f^2 d \int_0^\infty \frac{(kd)^l}{\omega_k^2} J_m(kr) \exp\left(-\tfrac{1}{2}k^2d^2\right) dk. \qquad (36)$$

In the examples of section 3, these limiting states were reached within about 4 hours (See Fig. 8).

We use the limiting value of the wind or height at the centre of the perturbation divided by its initial value as a measure of the extent to which the perturbation is retained. For the special cases considered in section 3, this parameter can be expressed in terms of the integral

$$C_n = \int_0^\infty \frac{x^n}{1+\lambda x^2} \exp\left(-\tfrac{1}{2}x^2\right) dx \qquad (37)$$

where λ is a dimensionless form of the equivalent geopotential Φ defined by $\lambda=\Phi/(fd)^2$ and x is a dummy variable. For the three perturbations of Fig. 9 we find;

$$\left.\begin{array}{ll} \text{Zonal wind perturbation} & u_\infty/U = {}^1/_2\,\lambda\, C_3, \\ \text{Non-divergent wind perturbation} & u_\infty/U = {}^1/_2\,\lambda\, C_5, \\ \text{Height perturbation} & \phi_\infty/gh = C_1. \end{array}\right\} \quad (38)$$

Fig. 10 shows these functions plotted against λ for the range $0.01 < \lambda < 100$. At low values of λ (small equivalent depth or large spatial extent d) the wind perturbations settle down with greatly reduced intensity but the height perturbation is largely retained. Thus, the wind field adjusts to the height field. At large values of λ the reverse is true and the height field adjusts to the wind field. These results are in agreement with those of Temperton (1973) mentioned earlier, but our theoretical analysis extends his conclusions to perturbations of the height field and indicates the time scale and manner in which adjustment takes place.

The value of λ for our experiments (Φ = 8485 m, d = 400 km, latitude = 38.25°N) is 63.8, well into the range for which the height field adjusts to the wind field. Regarding this value as typical of analysis schemes used in numerical weather prediction, the difficulty of assimilating data from the mass field such as height or surface pressure observations is apparent. Most of the analysis increments are quickly lost in external gravity waves unless steps are taken to make corresponding adjustments to the wind field. Some additional loss of information may result from internal gravity waves not covered by the theory.

From experiments with various analysis schemes in a shallow water equation model, Daley and Puri (1980) also found difficulty in assimilating height information, especially when accompanied by wind data. Puri (1981) found that height data were much better retained if geostrophic wind

increments were also applied. Such increments are applied in our model when used operationally (Bell 1983, Atkins and Woodage 1985) but they were not applied in our perturbation experiments.

To explain the different levels at which the two wind perturbations of Fig. 9 settle, we look at the final state in more detail. In the general case of a local perturbation, the geopotential field tends to the following state found by integrating Eq. (12) between t=0 and t=∞ in accordance with (7).

$$\phi(r,\theta,\infty) = \phi(r,\theta,0) - \Phi \sum_{n=0}^{\infty} \int_0^{\infty} \frac{1}{\omega_k} \left(Q_n(k) \cos n\theta + S_n(k) \sin n\theta \right) J_n(kr)\, dk. \qquad (39)$$

This also determines the limiting wind field through the geostrophic relation. Eq. (39) involves the functions $Q_n(k)$ and $S_n(k)$ but not $P_n(k)$ or $R_n(k)$. These functions are given by Eqs. (15) and (16), from which it can be seen that the limiting steady state flow is independent of the initial divergence $D(r,\theta,0)$ and depends only on the initial geopotential field $\phi(r,\theta,0)$ and the ageostrophic vorticity $\alpha(r,\theta,0)$. If the initial perturbation includes a divergent wind, this component will be completely dispersed as a gravity wave and will have no effect on the steady state flow.

It can now be seen why the curve for the zonal wind perturbation in Fig. 9 tends to a value of 0.5 as λ increases. The initial wind field for this case can be resolved into divergent and rotational components of equal magnitude. As the divergent component contributes nothing to the residual flow, at least half of the perturbation is lost, regardless of the value of λ. In contrast, the curve for the non-divergent initial state in Fig. 9 tends to 100% retention of the initial field as λ increases.

In a study of the response of a shallow water equation model to different types of data, Daley (1980) came to similar conclusions. Assuming periodic behaviour, he found that a divergent wind field always tended to excite gravity waves rather than the Rossby waves which have the most significant impact on forecasts. A rotational wind field generally led to the opposite effect. The effect of a geopotential field depended on the horizontal scale and equivalent depth assumed; large-scale features or small equivalent depths being more effective in exciting Rossby waves rather than gravity waves. Daley's results were based on the projection of the initial conditions on the various wave modes of his equations at t=0, but their validity can be extended to the long term solution because of the weak interaction between Rossby and gravity waves.

6. Perturbations of Limited Depth

a. Theoretical analysis

The two-dimensional theory developed in section 2 applies to perturbations distributed uniformly throughout the depth of the atmosphere. An extension of this theory to the problem of perturbations covering a limited atmospheric depth would be a more accurate representation of the type of increments introduced into numerical models by the assimilation of single-level data. Even within the limitations of a linearised theory, the general problem is a difficult one owing to the baroclinic nature of the real atmosphere and the consequent excitation of internal gravity waves. We restrict consideration to the case of an isentropic atmosphere; i.e. one in which the potential temperature is the same at every point. This is clearly inappropriate for the stratosphere but may be regarded as a first approximation for the troposphere which will be the main area of interest.

In an atmosphere with a constant potential temperature, isentropic processes cannot alter the vertical temperature profile. The thickness between any two pressure levels will be constant, so that any perturbation in the height field will appear with equal

magnitude at all levels. The inability to generate any internal vertical structure in the height field simplifies the theory by precluding the generation of internal gravity waves. Perturbations can then decay only through external gravity waves as in the two-dimensional case.

The linearised equations of motion for the three-dimensional case are unchanged from Eqs. (1) and (2) although the wind components u and v will now be functions of pressure. The equations may be combined as before to yield Eqs. (5) and (6) in terms of divergence and vorticity. For the three-dimensional problem, Eq. (3) is replaced by

$$\frac{\partial p_s}{\partial t} + \int_0^{p_s} D \, dp = 0 \qquad (40)$$

which is just the continuity equation for a vertical column extending throughout the depth of the atmosphere. (The subscript s refers to a surface value.) In terms of the geopotential field, Eq. (40) can be written.

$$\frac{\partial \phi_s}{\partial t} + \frac{RT_s}{p_s} \int_0^{p_s} D \, dp = 0. \qquad (41)$$

We now express the variables D and ζ as the sum of a vertically averaged component indicated by an overbar, and a deviation from the vertical average indicated by an asterisk superscript. We have seen that the perturbation in the geopotential field is independent of level, so that ϕ is the same as the surface field ϕ_s, and ϕ^* is zero everywhere. Eq. (41) can then be written

$$\frac{\partial \bar{\phi}}{\partial t} + RT_s \bar{D} = 0. \qquad (42)$$

Taking the vertical average of Eqs. (5) and (6), we find

$$\frac{\partial \bar{D}}{\partial t} - f\bar{\zeta} + \nabla^2 \bar{\phi} = 0, \qquad (43)$$

$$\frac{\partial \bar{\zeta}}{\partial t} + f \bar{D} = 0. \qquad (44)$$

Equations (42) to (44) are identical in form to Eqs. (5) to (7) with the equivalent geopotential Φ replaced by RT_s. The solution for the vertically averaged flow is therefore identical to that for the two-dimensional case dealt with in previous sections with the equivalent depth given by

$$H = RT_s/g. \qquad (45)$$

This quantity is independent of the form of the perturbation or its vertical extent.

The solution for D^* and ζ^* can be found by subtracting equations (43) and (44) from (5) and (6) respectively giving

$$\frac{\partial D^*}{\partial t} - f \zeta^* = 0, \qquad (46)$$

$$\frac{\partial \zeta^*}{\partial t} + f D^* = 0, \qquad (47)$$

whose general solution can be written in complex form as

$$D^* + i \zeta^* = \left(D_0^* + i \zeta_0^* \right) e^{-ift} \qquad (48)$$

where the zero subscript refers to conditions at t=0. In terms of wind components this is equivalent to an inertial oscillation

$$u^* + iv^* = (u_o^* + iv_o^*)\, e^{-ift} \qquad (49)$$

which represents a wind field at each point of which the wind vector rotates with the coriolis frequency. Because the vertical integral of D^* vanishes, the wind field represented by (49) does not influence the height field. The oscillation therefore remains constant in magnitude because it cannot generate the gravity waves which would enable it to decay. In practice, beta-plane effects and baroclinic vertical structure permit the generation of internal gravity waves which eventually damp the oscillation. However, as the examples of the next section show, the damping is sufficiently slow for the theory to represent the main features of the early stages of the flow.

The wind oscillation of Eq. (49) added to the solution of Eqs. (42) to (44) constitutes the general solution for an isentropic atmosphere. If the initial wind perturbation can be separated into vertical and horizontal components, we can write

$$\underline{v}_o(r,\theta,p) = \underline{v}_o(r,\theta,p_r)\, F(p). \qquad (50)$$

Here $\underline{v}$ represents a horizontal wind vector and the zero subscript represents a value at t=0. F(p) is the vertical structure function and p_r is a reference pressure level. Although the general solution we have developed is not restricted to perturbations of this form, Eq. (50) represents the type of perturbation frequently generated by analysis schemes and will serve for the purposes of illustration. F(p) can be normalised so that its maximum value is unity, and a vertical mean $\overline{F}$ can be defined in the same way as $\overline{D}$ and $\overline{\zeta}$. The two-dimensional theory of section 2 is equivalent to $F(p) = \overline{F} = 1$.

Denoting the solution for the wind and potential fields in this case by $\underline{v}'(r,\theta,t)$ and $\phi'(r,\theta,t)$, the solution for the level-dependent case of Eq. (50) can be expressed as

$$\phi(r,\theta,p,t) = \bar{F}\,\phi'(r,\theta,t) \tag{51}$$

$$\underline{V}(r,\theta,p,t) = \bar{F}\,v'(r,\theta,t) + \left(F(p) - \bar{F}\right)\underline{V}_0(r,\theta,p_r)\,e^{-ift}. \tag{52}$$

To produce operational analyses, the numerical model uses a vertical structure function of the form

$$F(p) = \exp\left\{-3\,\ln^2(p/p_0)\right\} \tag{53}$$

where p_0 is the level of an observation being assimilated. If p_0 is in the middle or upper troposphere so that F(p) becomes insignificant at the ground, $\bar{F}$ may be approximated by

$$\bar{F} \approx \left(\frac{\pi}{3}\right)^{1/2} e^{1/12}\,p_0/p_s\,. \tag{54}$$

Through Eq. (52), $\bar{F}$ determines the fraction of the wind increment which excites the external gravity wave and geostrophic residual flow rather than the inertial wave. A perturbation applied to upper levels of the model therefore generates a larger inertial component than one at lower levels. In our analysis, this component does not decay, but in the atmosphere, decay takes place through internal gravity waves and non-linear effects. Although these decay processes operate more slowly than the initial adjustment in the two-dimensional problem, some deviation between numerical model runs and the theoretical analysis can be expected at an earlier stage than in section 4.

b. Model runs and results

To assess the validity of the foregoing analysis, further runs of the numerical model were performed with the zonal and non-divergent wind perturbations of section 3 but with different weights at each model level. These experiments were similar to those of Barwell and Lorenc (1985) but use the more recent 15-level model (Bell 1983). The perturbations used were those of Figs. 1(a) and 1(b) but with the central velocity increased to 20 m/s. They were applied at the same geographical location previously used (38.25°N, 150.94°W) with a vertical structure given by Eq. (53) with p_o = 257 mb. This level corresponded to one of the model levels at this location and is typical of levels at which aircraft observations are most abundant and generate the greatest impact on analyses and forecasts (Barwell and Lorenc 1985, Baede et al. 1985). The experiments can therefore be viewed as representing the effect of analysis increments due to an isolated single-level wind observation such as an aircraft report. As before, no initialization or other technique to suppress gravity waves was applied.

Figs. 11 and 12 show the differences at 257 mb between forecast fields from these experiments and the control forecast. The layout is the same as for Figs. 5 and 6. Equivalent analytic solutions from Eqs. (51) and (52) are shown in Figs. 13 and 14. In these two figures, the height fields are identical with those of Figs. 2 and 3 scaled by a factor of $2\bar{F}$ (the '2' allows for the doubled magnitude of the initial perturbation). From Eq. (54), the appropriate value of $\bar{F}$ for these experiments is 0.2779.

Although the general level of agreement between the model runs and the analytical solution is not as good as before, the external gravity waves are well predicted both in form and velocity of propagation. (This would not have been the case if the two-dimensional theory had been used with a reduced equivalent depth to allow for the limited vertical extent of the perturbation.) After

the gravity wave has propagated away, the model runs generate more intense double-vortex patterns in the height fields than the theory predicts. The reason for this is not clear but is probably related to details of the atmospheric temperature structure, particularly as 257 mb is close to the tropopause. At both 100 and 500 mb (not shown) the magnitudes of the vortices are much closer to the theoretical values for at least the first four hours. At the lower level, the agreement in magnitude persists throughout the 18-hour forecast, but after a few hours, the 100 mb height field begins to decay through internal gravity waves, easily identified by their absence at other levels and low velocity of propagation. This process occurs more quickly in the stratosphere because the temperature structure differs from the isentropic profile assumed by the theory. Similar decay only becomes significant in the troposphere later in the forecasts.

With the physical parameters used above, Eq. (52) shows that at 257 mb, 72% of the wind perturbation forms the inertial oscillation, which has a period of about 19.3 hours corresponding to the coriolis frequency at 38.25°N. Because of its large amplitude, the inertial components are clearly seen in Figs. 11 to 14. At other levels the magnitude of this component is less, passing through zero at around 495 and 134 mb where the function (53) has its mean value.

7. Implications for assimilation schemes

External gravity waves represent spurious high-frequency noise in a numerical model. Two techniques used in assimilation schemes for minimising this noise are initialization and repeated insertion of data. These are effective in controlling the overall level of noise, but both have their drawbacks. Initialization by a method such as the non-linear normal mode technique (Williamson and Temperton 1981) can impair the fit of analysis to data and, unless special measures are taken, can degrade diabatically driven circulations such as the Hadley cell. Repeated insertion typically involves adding increments to a model at regular intervals over a period of several hours. The small increments used prevent the build-up of large amplitude gravity waves, but other

undesirable effects can occur. Fig. 9 shows that the initial adjustment occurs within a few hours, i.e. within the repeated insertion period. In fact, the height perturbation changes sign after about 30 minutes and stays negative until 2 hours. In a scheme in which the sizes of increments are calculated at each time step, this can lead to spurious increases in analysis increments during later stages of the assimilation. Barwell and Lorenc (1985) also point out that repeated insertion can interact with advection to produce excessive corrections to fields just downstream from the region where the increments are applied.

Section 5 pointed out the undesirable property of a divergent wind field in exciting external gravity waves, and also the difficulty of assimilating mass field data as shown by Figs. 8 and 10. Because the flow tends to adjust to the rotational wind field, the divergent wind is completely lost and the mass field almost completely lost during the early stages of the adjustment. For the mass field, the effect is most significant in the tropics and is controlled by the parameter λ (see Fig. 10). With values of λ typical of increments added by data assimilation schemes, adjustment of the mass field to the wind field is still a good approximation even in the polar regions. Clearly, some special treatment, such as the addition of geostrophic wind increments mentioned earlier, is essential for retaining height increments. Alternatively, a more complex multivariate analysis scheme (e.g. Lorenc 1981) can be used but Williamson et al. (1981) found that even multivariate optimum interpolation with non-linear normal mode initialization causes imbalance through use of the geostrophic relationship.

The suppression of undesirable gravity waves in models has been the subject of much study, but the inertial oscillation referred to above has received less attention. This may be partly because it lies outside the scope of two-dimensional shallow water theory, being a consequence of non-uniform vertical structure in the perturbations. Nevertheless, like fast gravity waves, it represents a spurious feature to be avoided in numerical analyses. The oscillation is more prominent for perturbations inserted in the upper atmosphere, especially those with a small vertical extent. It is set up quickly within the first few hours of adjustment but

decays much more slowly, largely through internal gravity waves. An inertial oscillation from the assimilation of an isolated aircraft observation can persist in a forecast for more than 24 hours and still retain much of its initial intensity. For most latitudes this represents more than one cycle of the oscillation. The problem is most serious at upper levels where a larger fraction of the initial wind increment is channelled into the oscillation. Much of the single-level observational data available for numerical weather prediction is obtained at these levels. Analysis of stratospheric wind data is particularly difficult because, with the much greater vertical gradient of potential temperature, decay through internal gravity waves is more rapid.

8. Summary

The linearised shallow water equations on an f-plane have been solved for a localised perturbation. Instead of assuming solutions periodic in both space and time, non-periodic solutions for isolated perturbations have been investigated. This was achieved by using local polar rather than cartesian co-ordinates in the plane and solving the equations using the method of separation of variables. A general solution has been found in the form of a series of terms involving Bessel functions, which can be fitted to any specified initial conditions. The solutions have been illustrated with examples of perturbations typical of those introduced into numerical models during data assimilation or intervention.

The solutions display an external gravity wave that forms and propagates outward from the perturbation site in the first few hours of the adjustment. This wave eventually separates from the residual flow which settles into a geostrophically balanced steady state. Comparison with experiments in which similar perturbations were applied to all levels of a numerical model indicates that the main features of the initial adjustment process and residual steady state are well represented. The magnitude and propagation velocity of the external gravity wave are particularly well predicted. The influence of internal gravity waves, not represented by the theory, does not cause serious disagreement with the theoretical analysis for the first 12 to 18 hours.

The two-dimensional theory was extended to the case of a perturbation whose magnitude was level-dependent. With the assumption of an isentropic temperature profile, a third component of the flow appears in addition to the external gravity wave and the geostrophic steady state. This is an inertial oscillation in the portion of the wind field which deviates from the vertically averaged wind. Internal gravity waves are still outside the scope of this extended theory but experiments indicate that they do not seriously invalidate the analysis, except in the stratosphere.

The work reported here sheds more light on the way that the process of adjustment occurs. The main conclusions from the theoretical analysis of the shallow water equations can be summarised in the following statements. In particular, the first is a more precise statement of the frequently used result that the 'height field adjusts to the wind field'.

i. The height field adjusts to the rotational component of the vertically averaged wind field

This result is a good approximation with the equivalent depth and spatial scales typical of assimilation schemes used in numerical models, although is not a general property of solutions to the shallow water equations. It supports the conclusion of various authors from experiments with numerical models that wind increments are better retained if only the rotational wind is updated.

ii. Unbalanced increments in the height field are almost completely dispersed by the external gravity wave

Like the previous result, this is a good approximation to the situation in typical numerical models but is not a general property of the equations. The retention of height increments is more difficult than wind increments and some special procedure to induce balancing is essential. Among the options available are the use of a multivariate assimilation scheme and the application of geostrophic wind increments.

iii. The divergence of the vertically averaged wind increments is completely dispersed by the external gravity wave

Thus, increments to the vertical mean divergence only contribute to unwanted gravity wave noise. In a numerical model, divergence damping or some procedure to eliminate the mean divergence is therefore beneficial. However, if applied to each individual level rather than the vertical average, divergence damping can impair the representation of features of the real atmosphere in which the divergence is important such as the Hadley cell circulation.

iv. The deviation of the wind increment from its vertical average initiates an inertial oscillation

This part of the wind field is not initially in balance with the height field. Furthermore, as it does not subsequently interact with the height field, there is no tendency toward a balanced state. An inertial oscillation with the coriolis frequency is therefore set up. The effect is most noticeable for wind increments in the stratosphere or upper troposphere, especially if applied through only a small pressure range. In an isentropic atmosphere, the oscillation is preserved indefinitely but in a more realistic atmospheric temperature profile, it decays slowly through internal gravity waves.

These results extend and place on a firmer theoretical foundation the results from two-dimensional theories. They are supported by the results of experiments with numerical models and are relevant to the design of analysis schemes, particularly with regard to constraints used to maintain the balance between mass and wind fields.

REFERENCES

Arakawa, A 1984: Geostrophic adjustment in continuous and discrete cases. WMO Short and Medium Range Weather Prediction Research Publication Series, No. 8, 25-41.

Atkins, M J and Woodage, M J 1985: Observations and data assimilation. Met. Mag., 114, 227-233.

Baede, A P M, Källberg, P and Uppala, S 1985: Impact of aircraft wind data on ECMWF analyses and forecasts during the FGGE period, 8-19 November 1979. ECMWF Tech. Rep. No. 47.

Balgovind, R, Dalcher, A, Ghil, M and Kalnay, E 1983: A stochastic-dynamic model for the spatial structure of forecast error statistics. Mon. Wea. Rev., 111, 701-722.

Barwell, B R and Lorenc, A C 1985: A study of the impact of aircraft wind observations on a large scale analysis and numerical weather prediction system. Quart. J. R. Met. Soc., 111, 103-129.

Bell, R S 1983: The Meteorological Office operational global data assimilation and forecast system. 6th Conf. on Numerical Weather Prediction, Omaha, Nebraska, June 6-9 1983, 269-274.

Blumen, W 1972: Geostrophic Adjustment. Rev. Geophys. Space Phys., 10, 485-528.

Cahn, A 1945: An investigation of the free oscillations of a simple current system. J. Met., 2, 113-119.

Daley, R 1980: On the optimal specification of the initial state for deterministic forecasting. Mon. Wea. Rev., 108, 1719-1735.

Daley, R and Puri, K 1980: Four-dimensional data assimilation and the slow manifold. Mon. Wea. Rev., 108, 85-99.

Erdélyi, A (ed.) 1954: Tables of integral transforms. McGraw-Hill Book Co.

Gadd, A J 1985: The 15-level weather prediction model. Met. Mag., 114, 222-226.

Gill, A E 1980: Some simple solutions for heat-induced tropical circulation. Quart. J. R. Met. Soc., 106, 447-462.

Heckley, W A and Gill, A E 1984: Some simple analytical solutions to the problem of forced equatorial long waves. Quart. J. R. Met. Soc., 110, 203-217.

Hollingsworth, A and Lönnberg, P 1986: The statistical structure of short-range forecast errors as determined from radiosonde data. Part I: The wind field. Tellus, 38A, 111-136.

Leith, C E 1980: Nonlinear normal mode initialization and quasi-geostrophic theory. J. Atmos. Sci., 37, 958-968.

Lönnberg, P and Hollingsworth, A 1986: The statistical structure of short-range forecast errors as determined from radiosonde data. Part II: The covariance of height and wind errors. Tellus, 38A, 137-161.

Lorenc, A C 1981: A global three-dimensional multivariate statistical interpolation scheme. Mon. Wea. Rev., 109, 701-721.

Puri, K 1981: Local geostrophic wind correction in the assimilation of height data and its relationship to the slow manifold. Mon. Wea. Rev., 109, 52-55.

Tanaka, H 1984: Time integration of shallow water equations in the gravity wave regime. J. Met. Soc. Japan, 62, 199-214.

Temperton, C 1973: Some experiments in dynamic initialization for a simple primitive equation model. Quart. J. R. Met. Soc., 99, 303-319.

Williamson, D L, Daley, R and Schlatter, T W 1981: The balance between mass and wind fields resulting from multivariate optimal interpolation. Mon. Wea. Rev., 109, 2357-2376.

Williamson, D L and Temperton, C 1981: Normal mode initialization for a multilevel grid-point model. Part II: Nonlinear aspects. Mon. Wea. Rev., 109, 744-757.

FIGURE CAPTIONS

Fig. 1 Idealised local wind and height perturbations. Isotachs (dotted) are shown every 2 m/s; contours (full lines) every 10 m.

Fig. 2 Response of analytical two-dimensional model to the zonal wind perturbation of Fig. 1(a). Charts are shown for 1, 2, 3 and 6 hours. Contours (full lines) are shown at 8 m intervals and isoatchs (dotted) every 2 m/s.

Fig. 3 As Fig. 2 for the non-divergent wind perturbation of Fig. 1(b) after 1, 2 and 4 hours.

Fig. 4 As Fig. 2 for the height perturbation of Fig. 1(c) after 1, 2, 3 and 6 hours. Contours are drawn at 4 m intervals.

Fig. 5 Response of a numerical model to the zonal wind perturbation of Fig. 1(a) applied at 38.25°N, 150.94°W with the same magnitude at all model levels. Charts are shown for 500 mb; those for other levels are similar. Times and isopleth intervals are the same as in Fig. 2.

Fig. 6 As Fig. 5 for the non-divergent wind perturbation of Fig. 1(b). Times and isopleth intervals are the same as in Fig. 3.

Fig. 7 As Fig. 5 for the height perturbation of Fig. 1(c). Times and contour intervals are the same as in Fig. 4.

Fig. 8 Wind speed or height at the centre of the perturbation expressed as a fraction of the value at t=0. Full lines represent analytical values; symbols represent values from numerical model experiments.

Fig. 9 Limiting flow as $t \to \infty$ in the analytical model for the three perturbations of Fig. 1. Contours are drawn every 4 m in (a) and (b) and 1 m in (c); isotachs are drawn every 4 m/s in (a) and (b) and 0.1 m/s in (c). The horizontal scale of the charts is the same as in Fig. 1.

Fig. 10 Fraction of the initial perturbation retained as $t \to \infty$ plotted against λ ($= \Phi/(fd)^2$) for the three types of perturbation shown in Fig. 1.

Fig. 11 Response of a numerical model to a zonal wind perturbation applied at each level with a non-uniform vertical structure function. The initial perturbation had a magnitude of 20 m/s (i.e. twice that of Fig. 1(a)) and was also weighted with the function $\exp(-3 \ln^2(p/p_o))$ where p is pressure and p_o the level of the maximum perturbation. In this example, p_o = 257 mb. Charts are shown for the response at 257 mb after 1, 2, 3 and 6 hours. Contours (full lines) are shown at 4 m intervals and isotachs (dotted) every 4 m/s.

Fig. 12 As Fig. 11 for the non-divergent wind perturbation of Fig. 1(b) applied with doubled intensity and with the same vertical structure function. Charts are shown for 257 mb after 1, 2 and 4 hours. Contours (full lines) are shown at 4 m intervals and isotachs (dotted) every 4 m/s.

Fig. 13 Response of the analytical model to a zonal wind perturbation applied with a non-uniform vertical structure function. The initial perturbation was as in Fig. 1(a) but with magnitude increased to 20 m/s and weighted with the function $\exp(-3 \ln^2(p/p_o))$ with p_o = 257 mb. Charts are for 257 mb; times and isopleth intervals are as for Fig. 11.

Fig. 14 As Fig. 13 for the non-divergent wind perturbation of Fig. 1(b) applied with doubled intensity and the same vertical structure function. Charts are for 257 mb; times and isopleth intervals are as for Fig. 12.

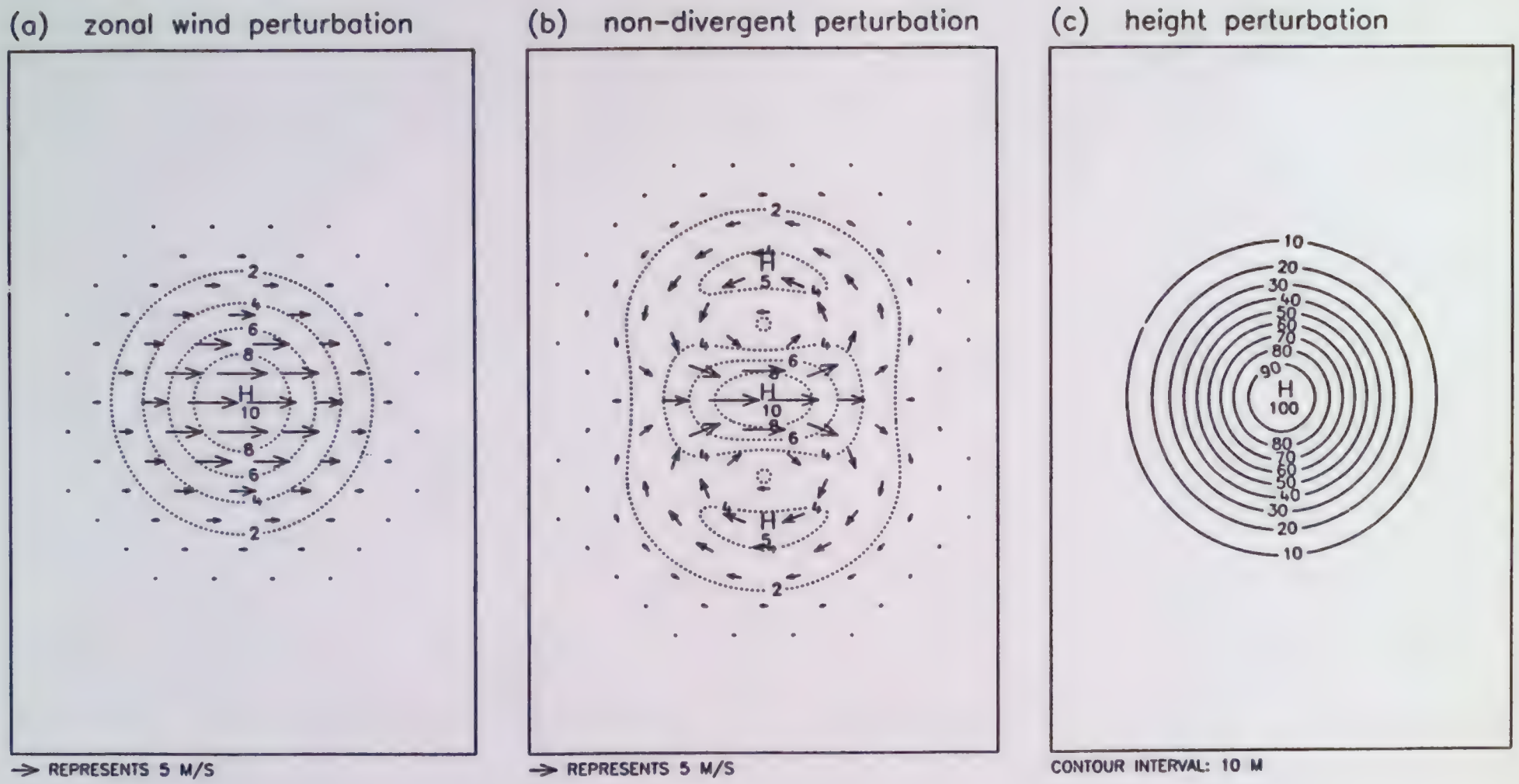

Fig. 1 Idealised local wind and height perturbations. Isotachs (dotted) are shown every 2 m/s; contours (full lines) every 10 m.

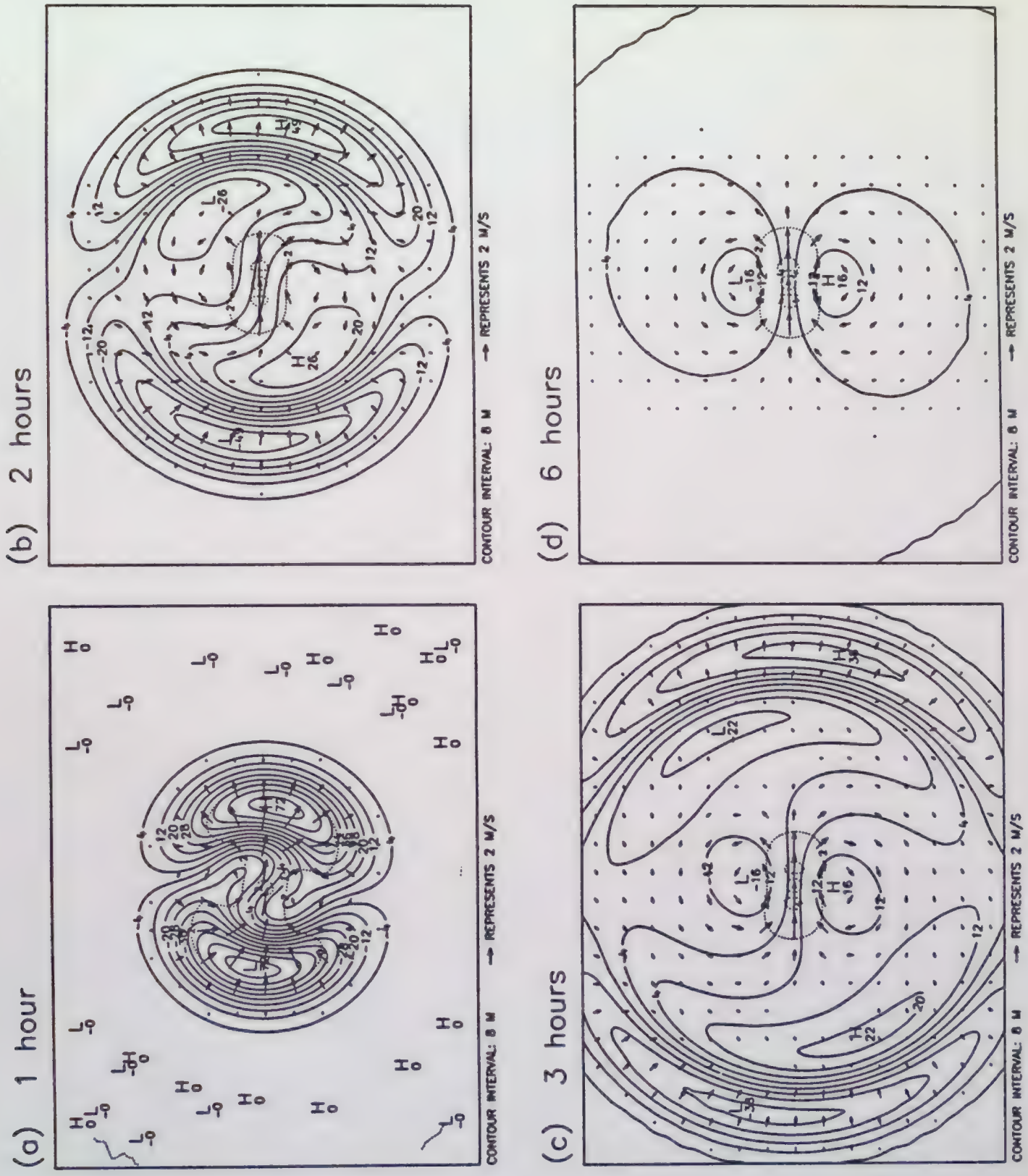

Fig. 2 Response of analytical two-dimensional model to the zonal wind perturbation of Fig. 1(a). Charts are shown for 1, 2, 3 and 6 hours. Contours (full lines) are shown at 8 m intervals and isoatchs (dotted) every 2 m/s.

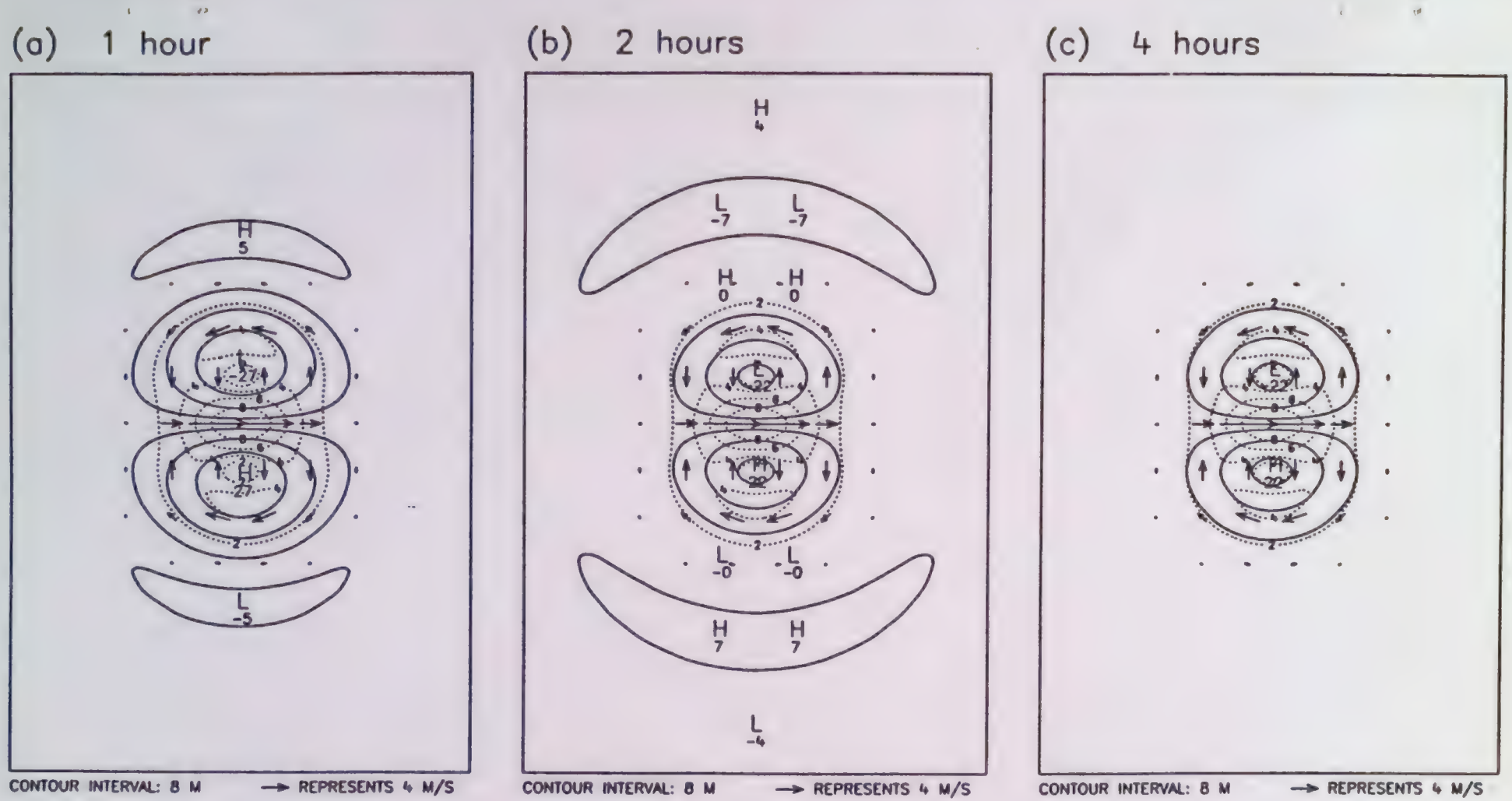

Fig. 3 As Fig. 2 for the non-divergent wind perturbation of Fig. 1(b) after 1, 2 and 4 hours.

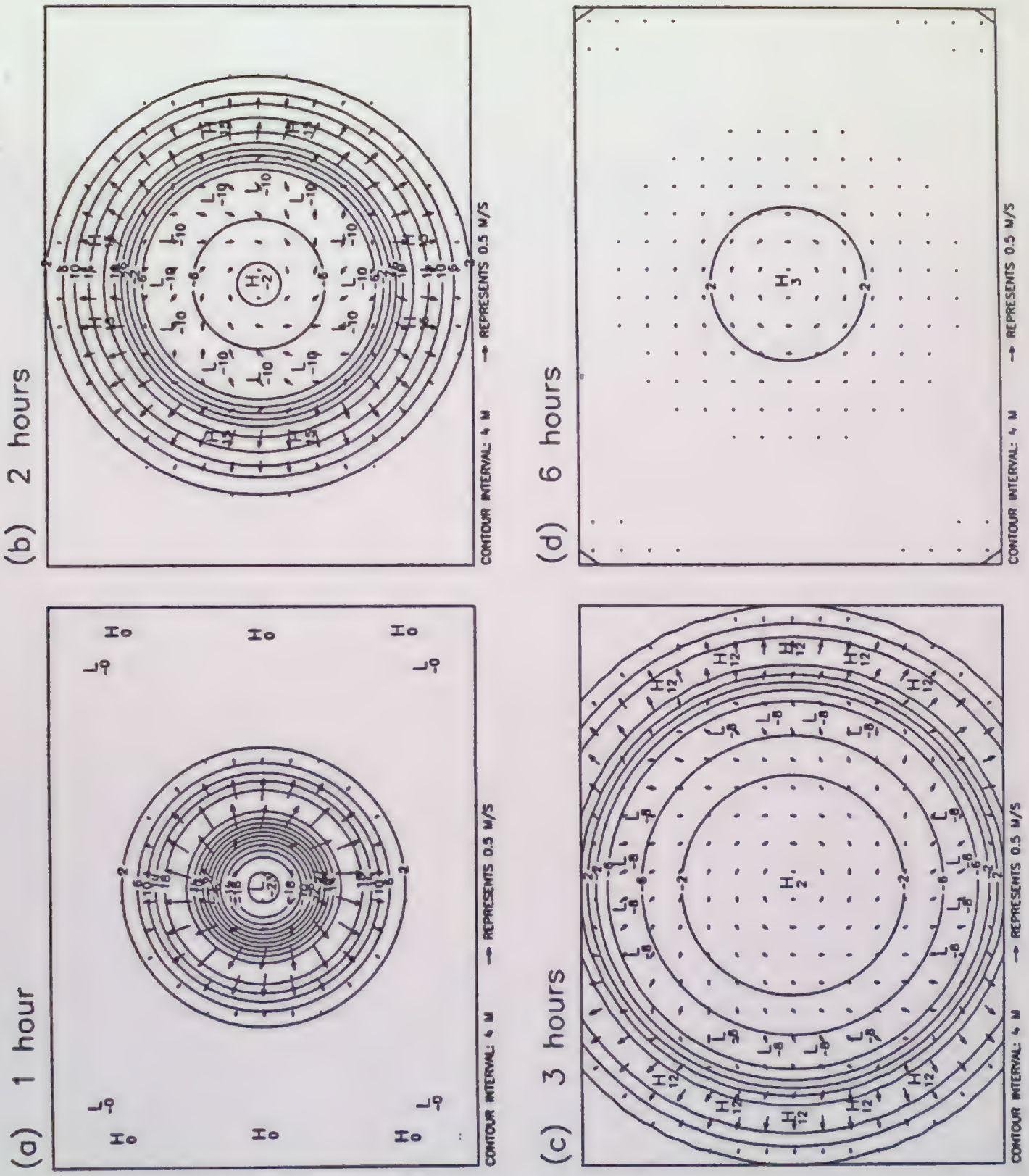

Fig. 4 As Fig. 2 for the height perturbation of Fig. 1(c) after 1, 2, 3 and 6 hours. Contours are drawn at 4 m intervals.

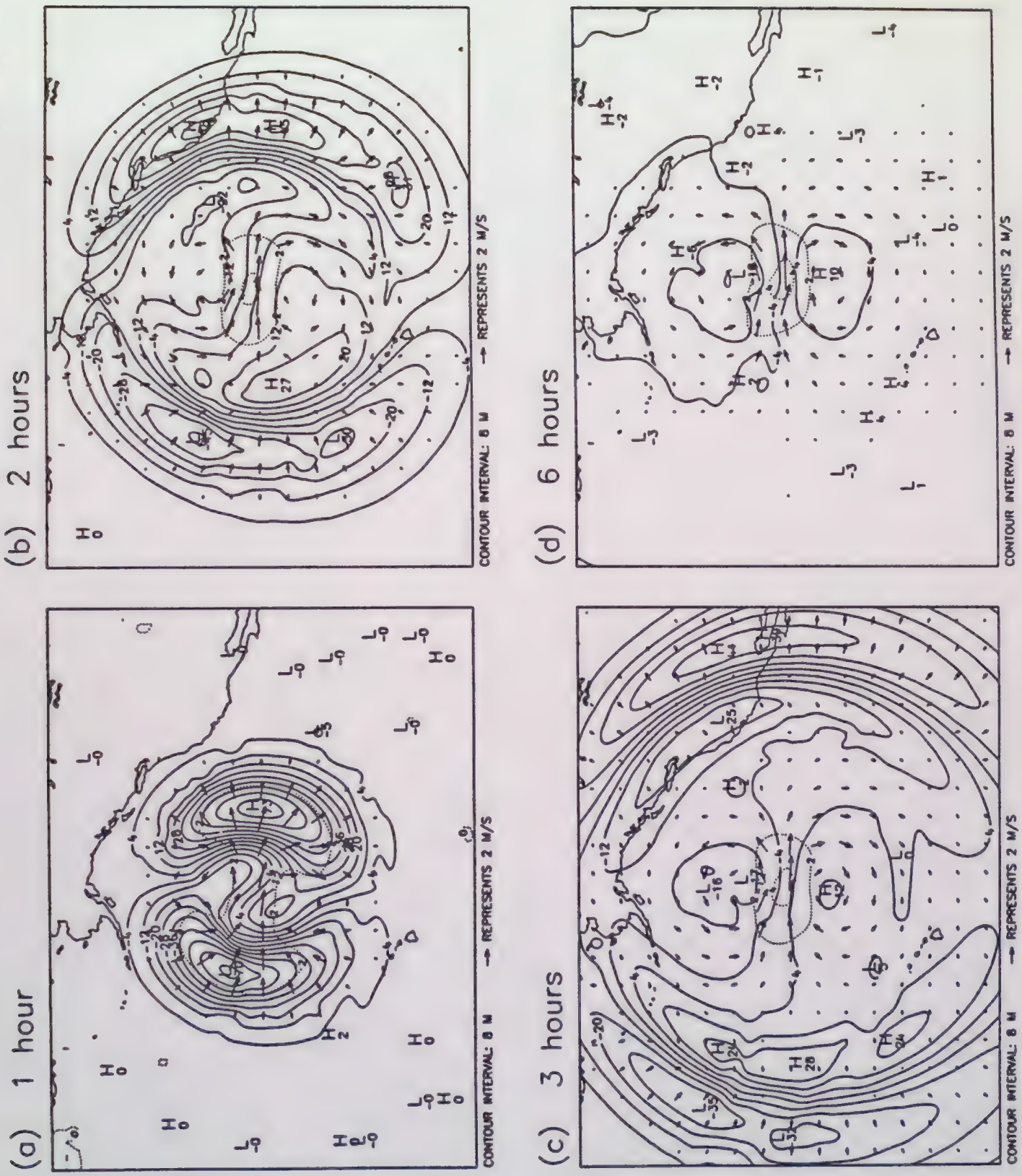

Fig. 5 Response of a numerical model to the zonal wind perturbation of Fig. 1(a) applied at 38.25°N, 150.94°W with the same magnitude at all model levels. Charts are shown for 500 mb; those for other levels are similar. Times and isopleth intervals are the same as in Fig. 2.

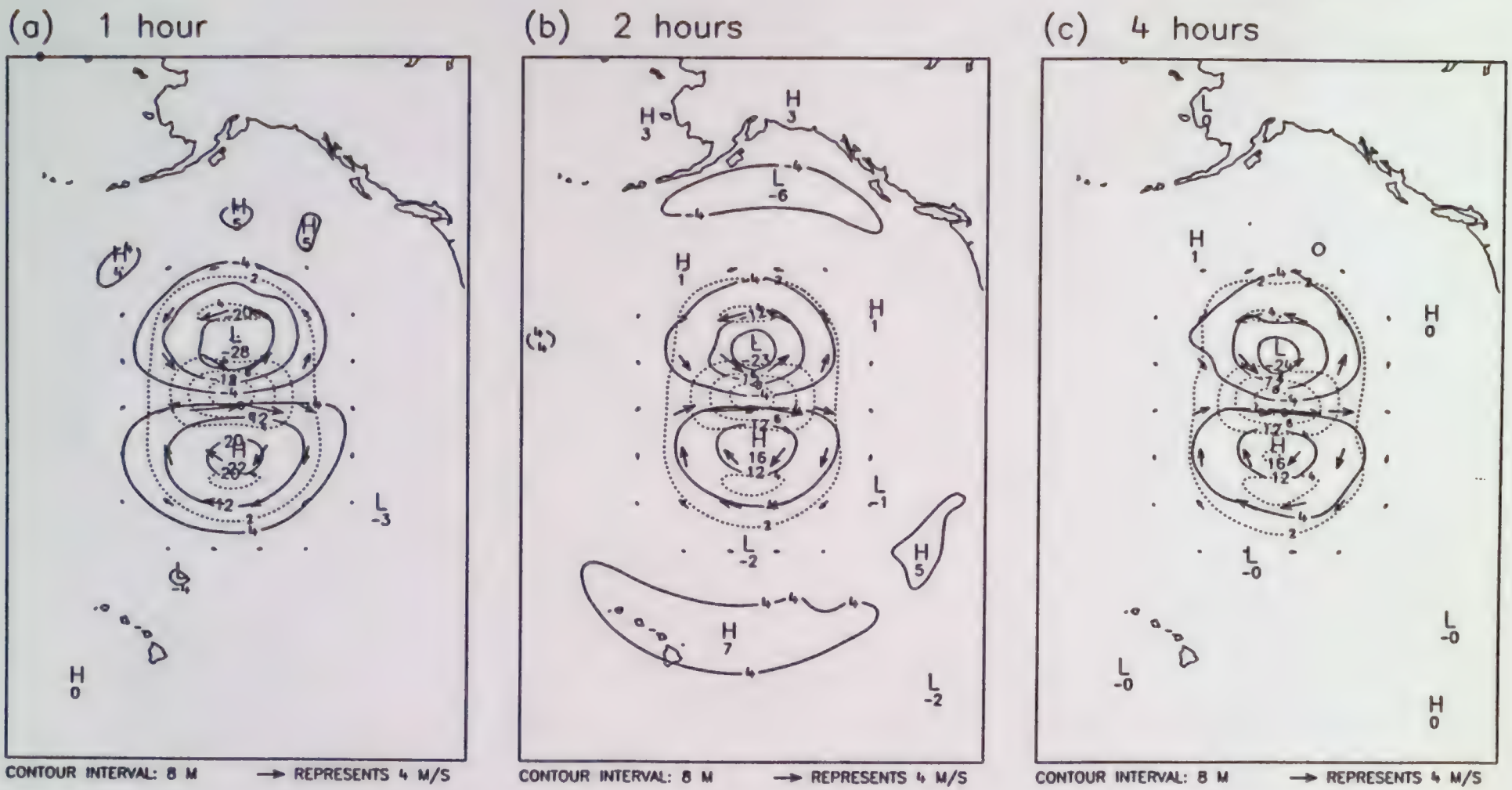

Fig. 6 As Fig. 5 for the non-divergent wind perturbation of Fig. 1(b). Times and isopleth intervals are the same as in Fig. 3.

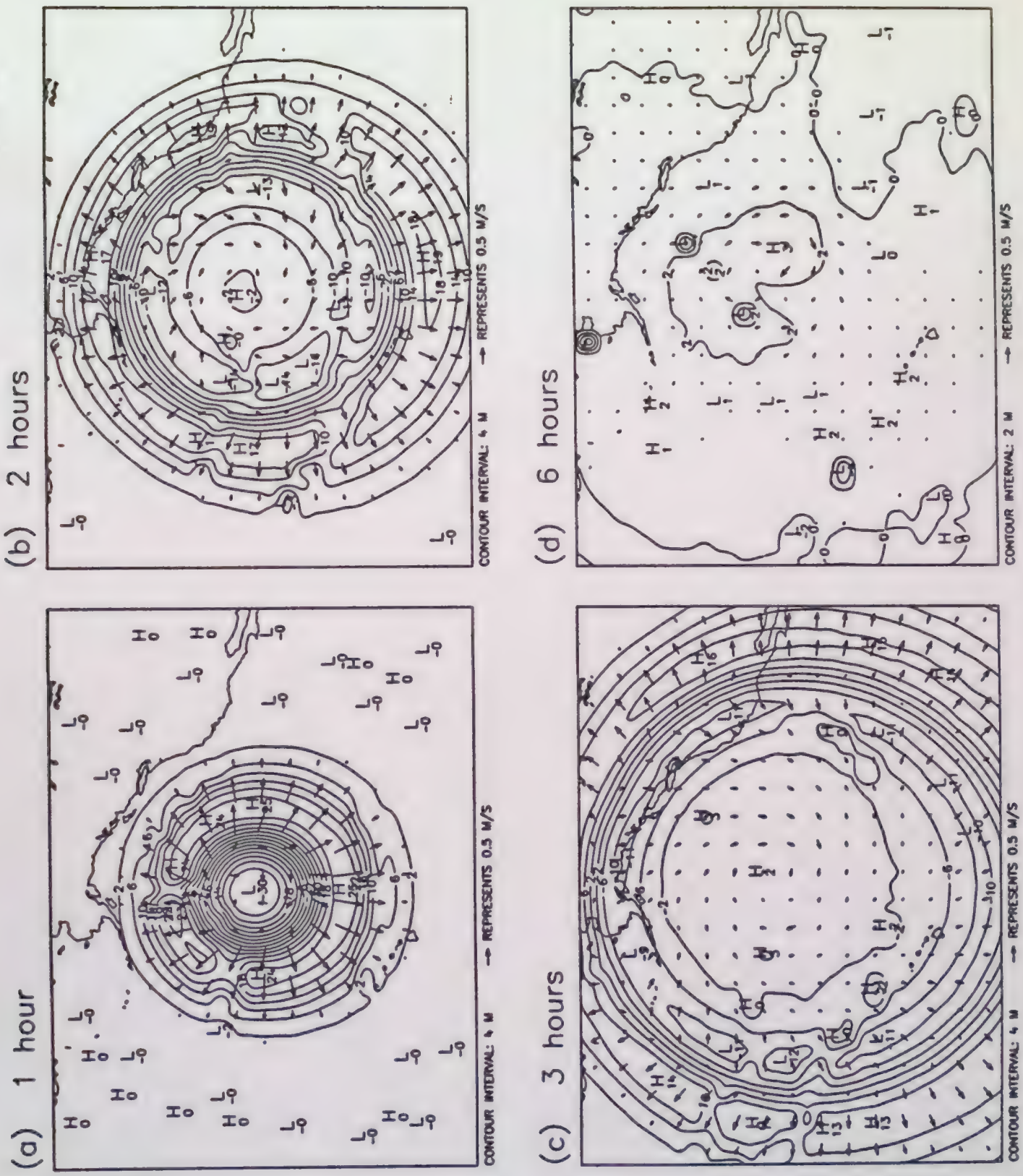

Fig. 7 As Fig. 5 for the height perturbation of Fig. 1(c). Times and contour intervals are the same as in Fig. 4.

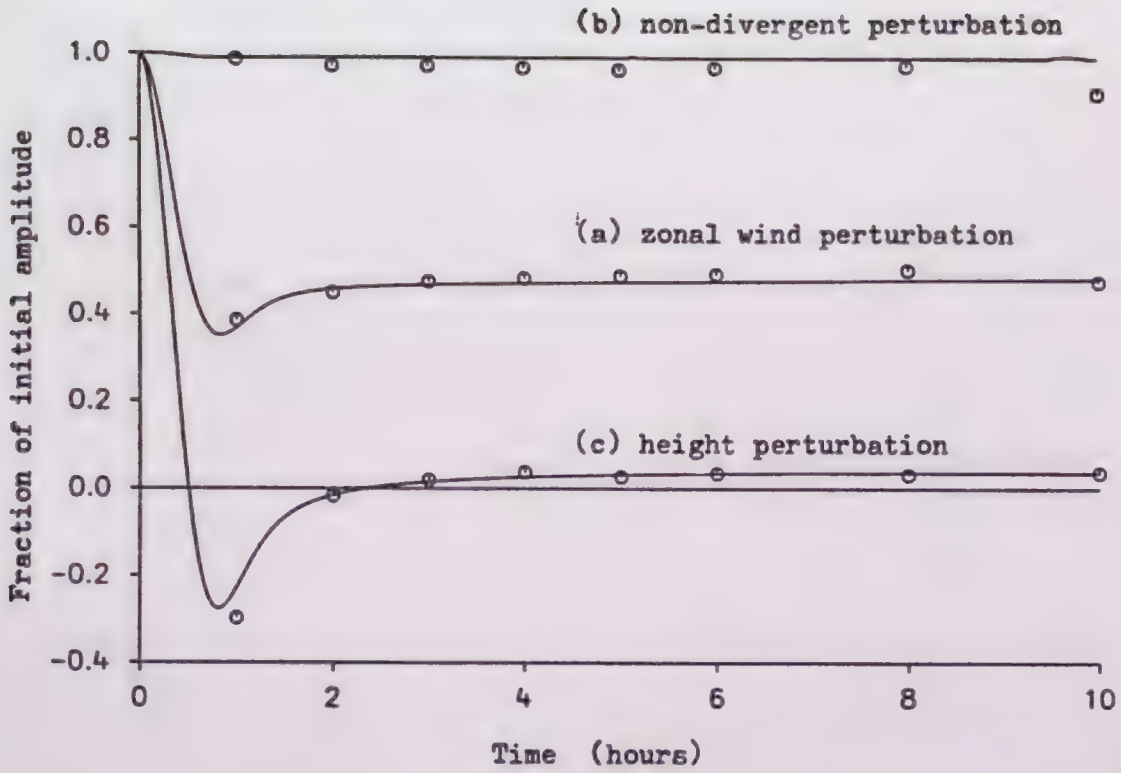

Fig. 8 Wind speed or height at the centre of the perturbation expressed as a fraction of the value at t=0. Full lines represent analytical values; symbols represent values from numerical model experiments.

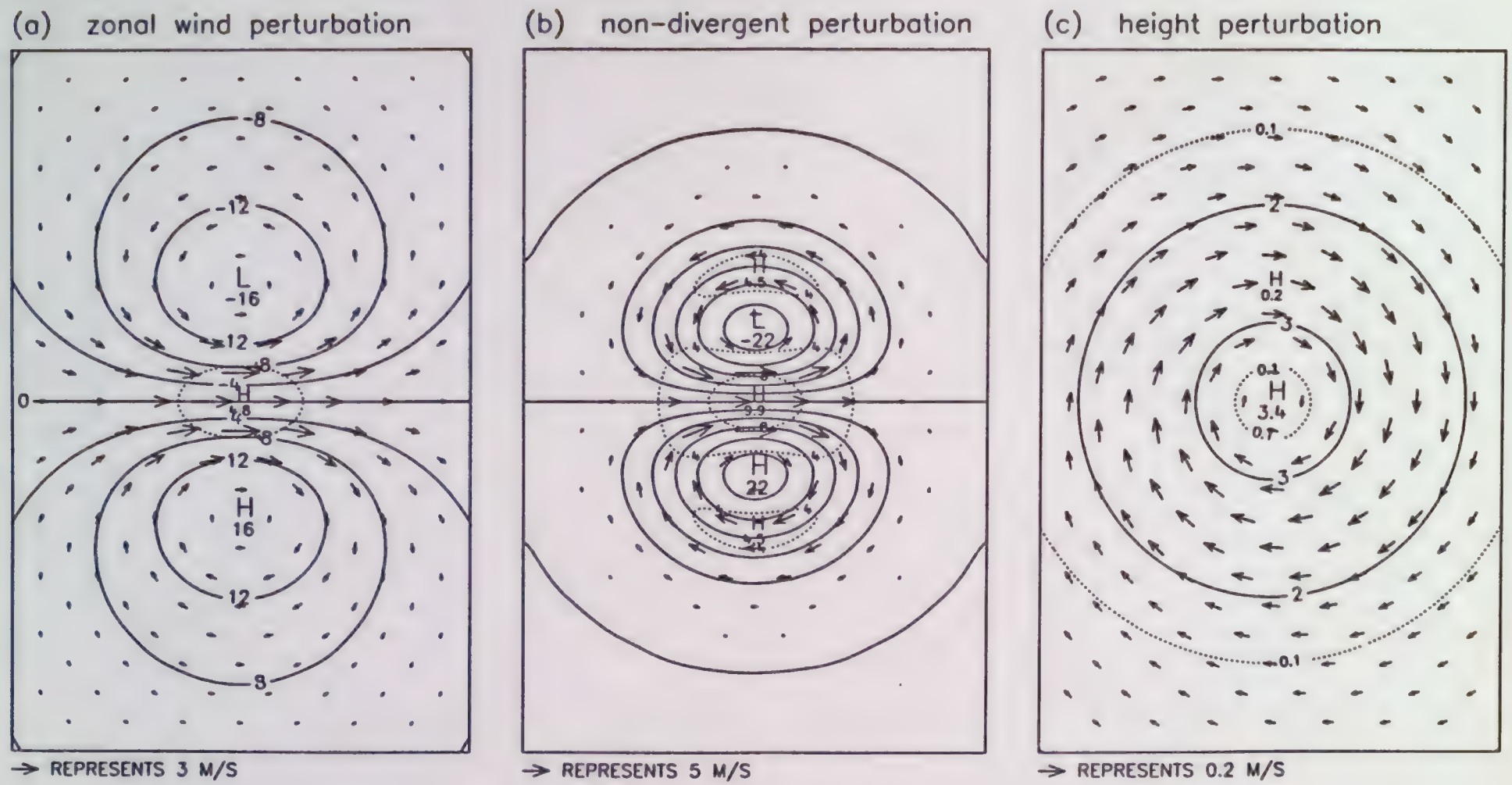

Fig. 9 Limiting flow as t→∞ in the analytical model for the three perturbations of Fig. 1. Contours are drawn every 4 m in (a) and (b) and 1 m in (c); isotachs are drawn every 4 m/s in (a) and (b) and 0.1 m/s in (c). The horizontal scale of the charts is the same as in Fig. 1.

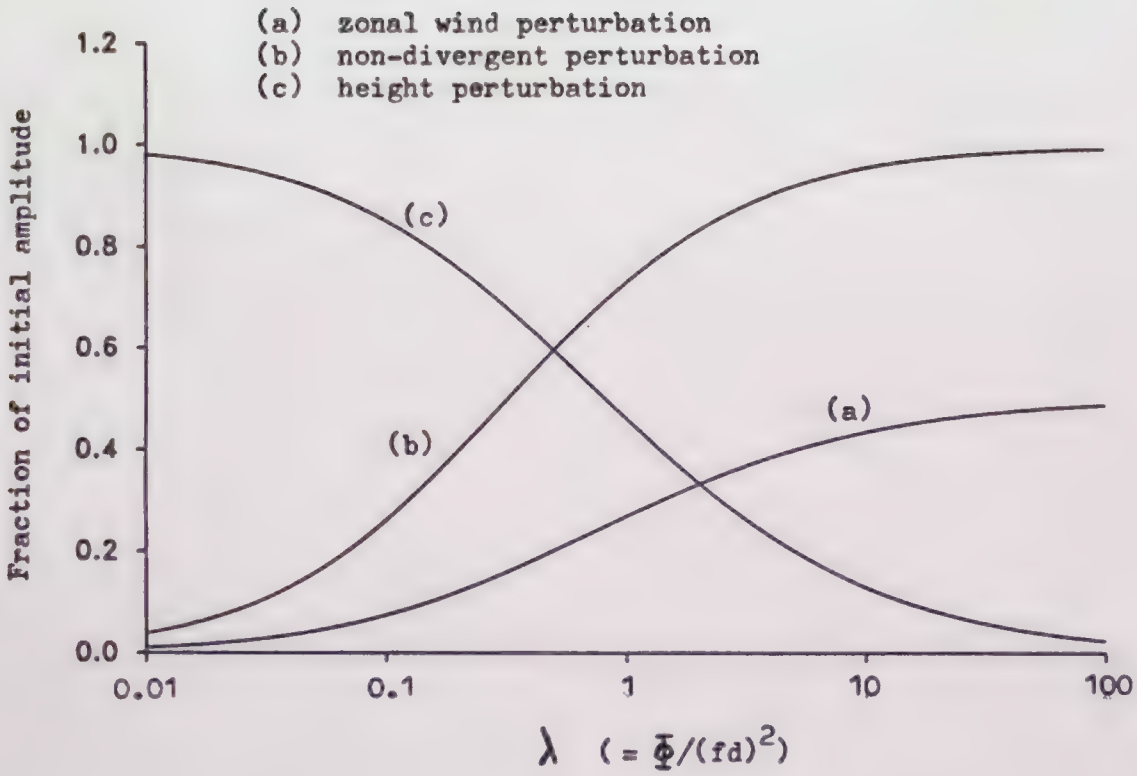

Fig. 10 Fraction of the initial perturbation retained as $t \to \infty$ plotted against λ ($= \Phi/(fd)^2$) for the three types of perturbation shown in Fig. 1.

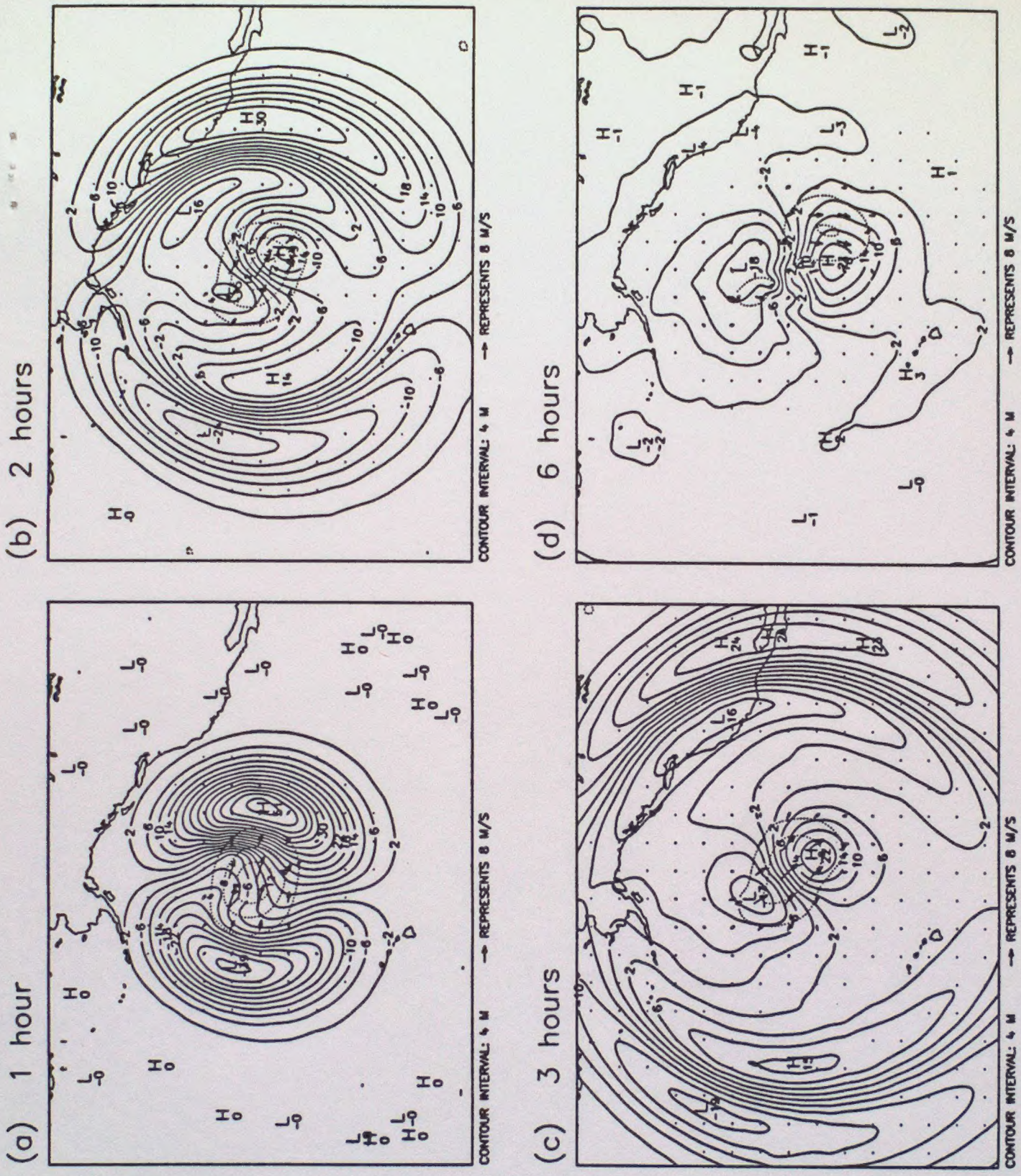

Fig. 11 Response of a numerical model to a zonal wind perturbation applied at each level with a non-uniform vertical structure function. The initial perturbation had a magnitude of 20 m/s (i.e. twice that of Fig. 1(a)) and was also weighted with the function exp $(-3 \ln^2(p/p_o))$ where p is pressure and p_o the level of the maximum perturbation. In this example, p_o = 257 mb. Charts are shown for the response at 257 mb after 1, 2, 3 and 6 hours. Contours (full lines) are shown at 4 m intervals and isotachs (dotted) every 4 m/s.

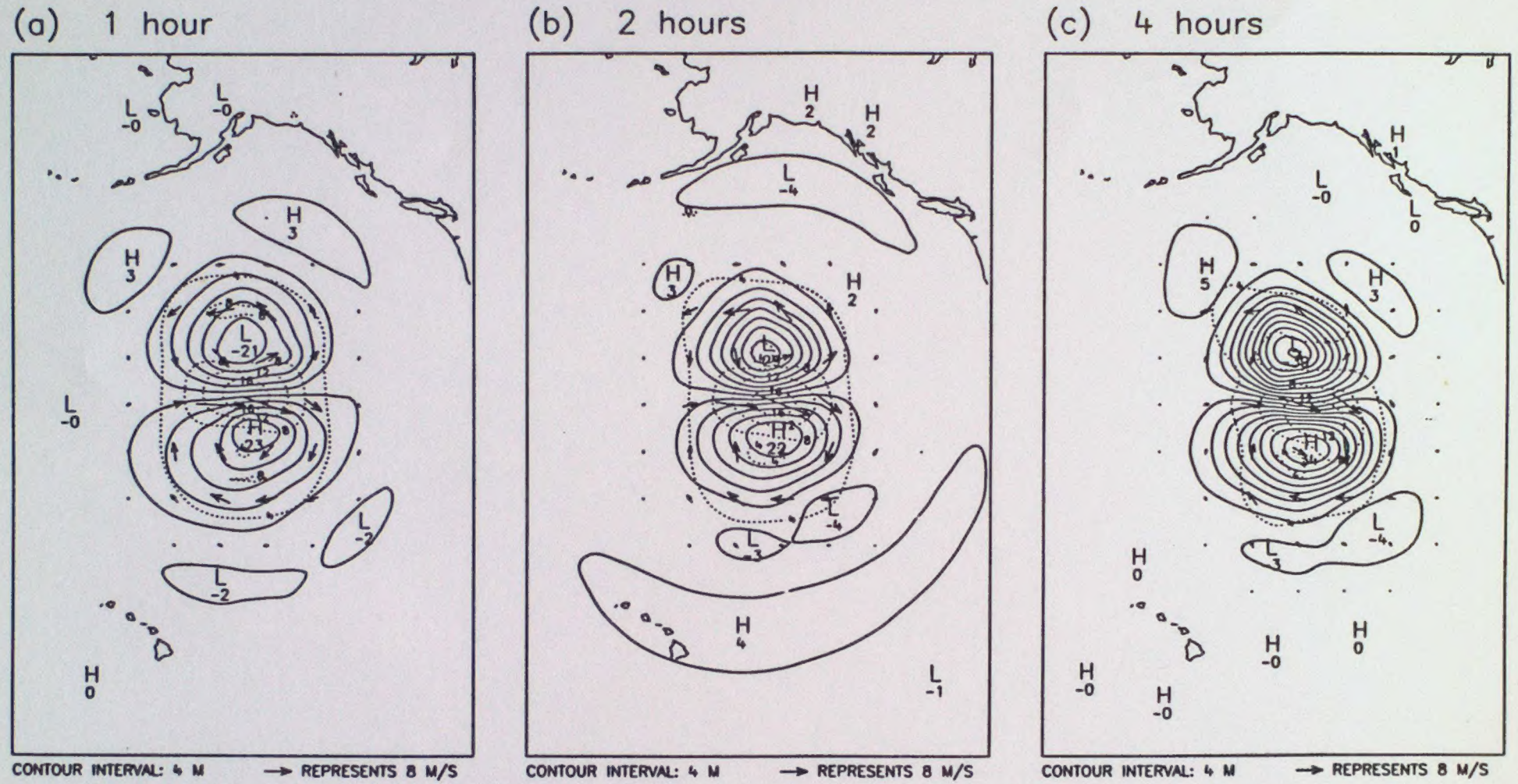

Fig. 12 As Fig. 11 for the non-divergent wind perturbation of Fig. 1(b) applied with doubled intensity and with the same vertical structure function. Charts are shown for 257 mb after 1, 2 and 4 hours. Contours (full lines) are shown at 4 m intervals and isotachs (dotted) every 4 m/s.

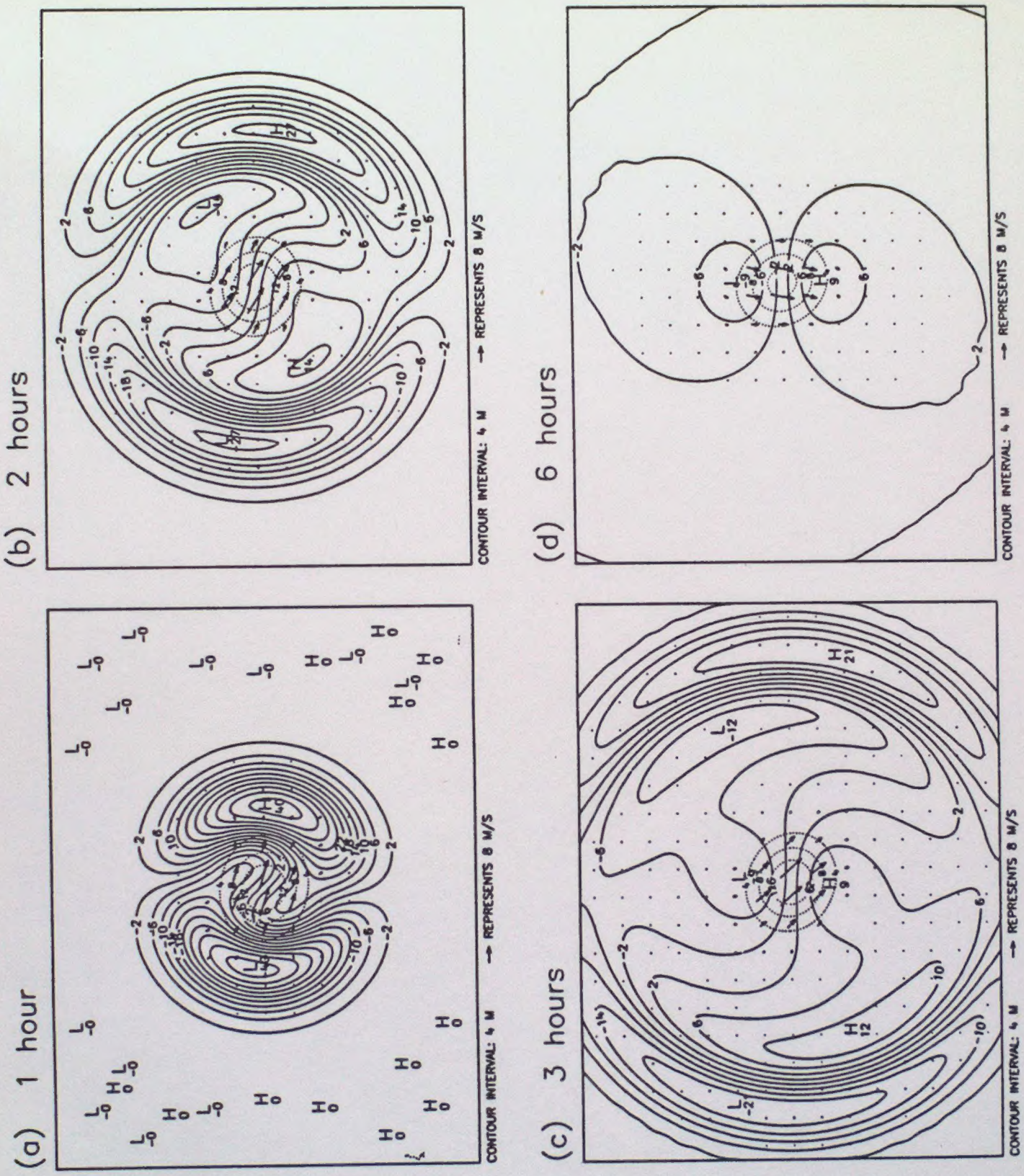

Fig. 13 Response of the analytical model to a zonal wind perturbation applied with a non-uniform vertical structure function. The initial perturbation was as in Fig. 1(a) but with magnitude increased to 20 m/s and weighted with the function $\exp(-3 \ln^2(p/p_o))$ with p_o = 257 mb. Charts are for 257 mb; times and isopleth intervals are as for Fig. 11.

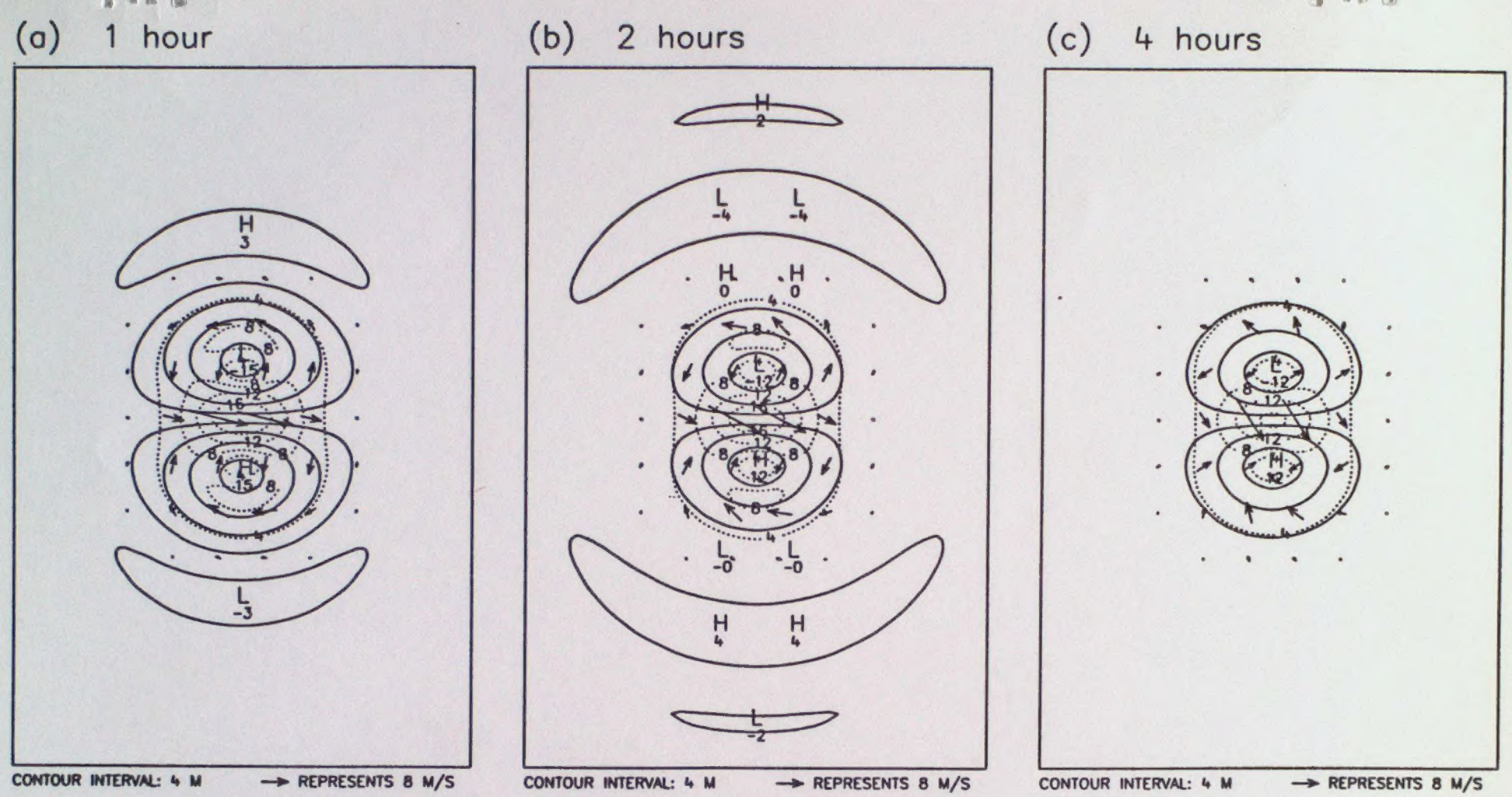

Fig. 14 As Fig. 13 for the non-divergent wind perturbation of Fig. 1(b) applied with doubled intensity and the same vertical structure function. Charts are for 257 mb; times and isopleth intervals are as for Fig. 12.